Journal of Solid State Chemistry 182 (2009) 1950–1963

Contents lists available at ScienceDirect

Journal of Solid State Chemistry

journal homepage: www.elsevier.com/locate/jssc

Materials discovery by crystal growth: Lanthanide metal containing oxides of the platinum group metals (Ru, Os, Ir, Rh, Pd, Pt) from molten alkali metal hydroxides

Samuel J. Mugavero III, William R. Gemmill, Irina P. Roof, Hans-Conrad zur Loye *

Department of Chemistry and Biochemistry, University of South Carolina, Columbia, SC 29208, USA

ARTICLE INFO

Article history:
Received 18 December 2008
Received in revised form
27 April 2009
Accepted 3 May 2009
Available online 12 May 2009

Keywords:
Crystal growth
Hydroxide flux
Platinum group oxides

ABSTRACT

This review addresses the process of materials discovery via crystal growth, specifically of lanthanide metal containing oxides of the platinum group metals (Ru, Os, Ir, Rh, Pd, Pt). It provides a detailed overview of the use of hydroxide fluxes for crystal growth. The melt chemistry of hydroxide fluxes, specifically, the extensive acid base chemistry, the metal cation solubility, and the ability of hydroxide melts to oxidize metals are described. Furthermore, a general methodology for the successful crystal growth of oxides is provided, including a discussion of experimental considerations, suitable reaction vessels, reaction profiles and temperature ranges. Finally, a compilation of complex platinum group metal oxides recently synthesized using hydroxide melts, focusing on their crystal growth and crystal structures, is included.

© 2009 Elsevier Inc. All rights reserved.

1. Introduction

The discovery of new materials and new properties has been the driving force in solid-state chemistry for many decades and has resulted in the synthesis and characterization of a plethora of new compounds. This statement can quickly be confirmed by looking at any one of the many structural databases covering solid-state compounds, such as the inorganic crystal structure database (ICSD) or the powder diffraction files (PDF). Interestingly, however, in doing so, one also notices that the number of new compounds quickly drops off as the number of constituent elements increases. In other words, we have become proficient at preparing compositions of relatively simple structures, but this ability has not typically extrapolated to the more complex compositions and structures. This is not meant as a slight on the solid-state chemist, but rather is a consequence of the traditional process of preparing new materials that is based on tried and true methods of chemical substitution. This is where the solid-state chemist shines—given a structure or composition as a starting point, he/she will immediately come up with numerous predictions of chemical substitutions that more often than not would result in new compositions and, sometimes, structures. These predictions often rely on radius ratio rules and on our understanding of oxidation states and coordination environment preference of the elements. For example, our group has investigated perovskite oxides for many years and has published structural predictions and approaches for making new compositions based on size, oxidation state preferences, and electronegativities [1,2]. All those approaches, however, work well only for binary and ternary phases, are troublesome for quaternary compositions, and are not yet developed for more complex compositions. Yet, it is believed that these more complex structures may hold the key to realizing some of the most desirable properties [3,4]. So, how does one discover complex compositions with new structures? In this review, we describe one approach, based on crystal growth from high temperature solutions that has proven to be an excellent route to the discovery of complex lanthanide containing platinum group metal oxides.

To introduce our approach and to explain our rationale for choosing it, we will draw on the concept of an "Energy Landscape" as described by Martin Jansen [5,6]. This concept stipulates that ALL compounds capable of existence are present on an energy landscape and that, furthermore, each composition capable of existence is associated with a local minimum on that landscape. A direct result of this mind-set is the concept of *discovery* rather than *creation* of a new material, as well as the implication that we are exploring this landscape by carrying out syntheses to find the local minima. Historically, we have had much success in identifying such minima, as demonstrated by the large number of new solid-state structures that are prepared each year. In fact, one can argue that we have been extraordinarily successful at locating these minima for simple compositions, but are struggling to extend our success to the more complex compositions.

* Corresponding author.
E-mail address: zurloye@mail.chem.sc.edu (H.-C. zur Loye).

0022-4596/$ - see front matter © 2009 Elsevier Inc. All rights reserved.
doi:10.1016/j.jssc.2009.05.006

The prediction of a structure for a new composition may often be accurately intuited if the synthesis involves a simple cationic substitution of a known composition. For example, given the spinel $ZnFe_2O_4$ as a starting point, we can readily predict that the substitution of Mg^{+2} (ionic radius 0.72 Å) for Zn^{+2} (ionic radius 0.73 Å), to yield the spinel $MgFe_2O_4$, is likely to succeed. In fact, for such simple structures we can do better; the knowledge of oxidation state specific ionic radii, such as the ones by Shannon and Prewitt [7] coupled with the concept of radius ratio rules [8] has enabled accurate predications of many simple structures with binary and ternary compositions, including rock salt (AO), rutile (AO_2), fluorite (AO_2), spinel (AB_2O_4), and perovskite (ABO_3), to name a few. Thus, for some of these structures we are quite capable of making predictions from scratch. By contrast, predicting the structure of a composition like $YBa_2Cu_3O_7$ ($AB_2C_3O_7$) (prior to its structure determination—of course) would be a challenge. The addition of a third cation, a third structural variable, opens up many more topological possibilities and we have difficulties predicting which one of the potential structures we have hypothesized will form, assuming, of course, that the correct structure is in fact among them. Moreover, we are faced with the conundrum of how to come up with this $AB_2C_3O_7$ composition in the first place in order to attempt a structural prediction. Of course, were we given the details of such a complex structure, we would be quite capable of predicting related compositions and, perhaps, could even anticipate minor structural deviations. Moreover, we could envision alterations to such compositions that would lead to the appearance of a desired functionality. This suggests that it would be most expedient for preparing new compositions with complex structure types (for example, as part of a project to target a specific property) if one were given a complex structure to start with. To address this issue, we have established one method, crystal growth from molten hydroxides that is most adept at resulting in the *discovery* of new compositions with complex structures.

2. Crystal growth from molten hydroxides

The use of high temperature solutions for crystal growth is well established [9] and, while crystals of most materials can be grown out of more than one solvent system, it is known empirically that some fluxes work especially well for some classes of materials. This is the case for hydroxide melts, which are believed to be one of the best solvent systems for oxides [10–12], corroborated by the fact that they have been used with great success for the crystal growth of a wide variety of complex oxides [13–24]. There are, of course, many reasons why hydroxide melts work so well for growing oxide crystals, including their low melt temperatures (Table 1) and extensive capacity for dissolving oxides; but more than any other is the adjustability of the acid–base chemistry of the hydroxide melt, which controls the solubility of metal cations. While it may seem counterintuitive to talk about an acid–base chemistry of a melt consisting of hydroxide ions, this concept of oxo-acidity was in fact described by Lux and Flood long ago [25,26].

The concept of oxo-acidity, which describes the chemical composition of a hydroxide melt, can best be appreciated by a comparison with the well known acid–base chemistry of water, where the auto-dissociation of water

$$2H_2O \rightleftarrows H_3O^+ \text{ (acid)} + OH^- \text{ (base)} \quad (1)$$

with an equilibrium constant, $K_w = 1\times10^{-14}$ at 25 °C, leads to an equilibrium concentration of $[H_3O^+] = [OH^-] = (K_w)^{1/2} = 1\times10^{-7}$, or in the familiar p-notation, pH = 7. If there is an excess of H_3O^+, then the pH < 7 and we talk about an acidic solution, or if there is an excess of OH^-, then the pH > 7 and we talk about a basic solution. The same process of auto-dissociation takes place in hydroxide melts [11,25–28]

$$2OH^- \rightleftarrows H_2O \text{ (acid)} + O^{2-} \text{ (base)} \quad (2)$$

with a dissociation constant, K_d, that depends on the identity of the metal cation—Li, Na, K, etc., which determines the equilibrium concentration of H_2O and O^{2-} at a given temperature. In this Lux–Flood concept of oxo-acidity, the acid is defined as an O^{2-} acceptor, while the base is defined as an O^{2-} donor; the "neutral" species being OH^-. An excess of H_2O will make the melt "acidic", while an excess of O^{2-} will make the melt "basic". To represent the acidity of any OH flux, we define $pH_2O = -\log[H_2O]$.

For Eq. (2), the dissociation constant $K_d = [H_2O][OH^-]$, where $[H_2O] = [OH^-] = (K_d)^{1/2}$ and $pH_2O = pO^{2-} = \frac{1}{2}pK_d$ = "neutral". Unlike in water, where there is a single dissociation constant, K_w, the value of K_d for a hydroxide melt is a function of the metal cation, Li, Na, K, etc., where the degree of dissociation typically increases with increasing charge density of the metal cation. Since Li^+ has the highest charge density of the alkali metals, LiOH, has the greatest degree of dissociation among the alkali metal hydroxides. Furthermore, the auto-dissociation process is endothermic and, therefore, the value of K_d increases with temperature. A graph showing the range of K_d values for several metal cations at different temperatures is depicted in Fig. 1, illustrating, that the equilibrium pH_2O values for different cations vary by many orders of magnitude [10,28,29].

The value of pH_2O affects the solubility of metals (oxides) and, thus, we can control the solubility of a given metal by choosing the specific hydroxide together with the flux temperature. In addition, we can physically add water to the melt, thereby increasing its acidity, or allow water to evaporate from the melt, thereby increasing its basicity. This gives us very powerful control over the melt chemistry, the pH_2O, and thus metal solubility, which makes hydroxide fluxes such outstanding media from which to grow complex oxide crystals. Once the "correct" pH_2O to achieve dissolution of several metals in a melt is found, a prerequisite for crystal growth, then the pH_2O can be altered, via temperature change (slow cooling) or water evaporation (open crucible), to induce a reduction in the solubility, leading to a controlled precipitation of a complex oxide in single crystal form.

The solubility of a metal oxide in a hydroxide melt depends on its mode of solvation or complexation in the hydroxide melt. Under acidic conditions,

$$M_2O_n(s) + nH_2O(sol) \rightleftarrows 2M^{n+}(sol) + 2nOH^- \text{ (l)} \quad (3)$$

Table 1
Melting points of the alkali metal hydroxides [28,156].

Hydroxide	Melting point (°C)	Eutectic composition (mol%)
LiOH	473	
NaOH	320	
KOH	400	
RbOH	301	
CsOH	272	
$Sr(OH)_2$	512	
$Ba(OH)_2$	409	
LiOH–NaOH	210	30:70
LiOH–KOH	226	31:69
NaOH–KOH	170	51:49
NaOH–RbOH	237	51:49
KOH–RbOH	306	65:35
LiOH–NaOH–KOH	167	9.5:49:41.5
NaOH–$Ba(OH)_2$	280	30:70
KOH–$Ba(OH)_2$	325	57:43

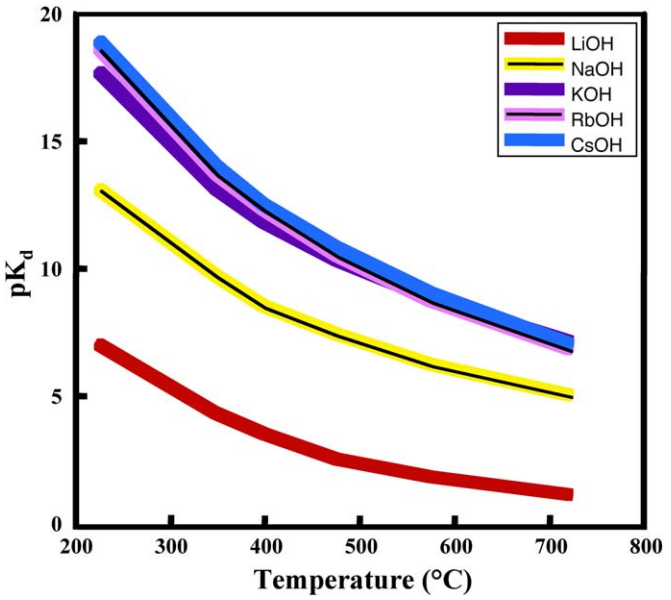

Fig. 1. Plot of the values of the auto-dissociation constant, pK_d, of molten alkali metal hydroxides over the temperature range 227–723 °C. Larger values of pK_d correspond to a lesser degree of melt dissociation. Please note that the data include theoretical values to extend the curves below the melting point of some hydroxides. These data are important for eutectic mixtures with melting points as low as 167 °C.

for example: Ln_2O_3 (s) + H_2O(sol) → $2Ln^{3+}$(sol) + $2O^{2-}$(sol) + 2 OH^-(sol).

The metal cation is solvated, while under basic conditions a metal oxo-anion is solvated.

$$M_2O_n(s) + mO^{2-}(sol) \rightleftarrows [M_2O_{n+m}]^{2m-}(sol) \quad (4)$$

for example: $Al_2O_3(s) + O^{2-}(sol) \rightarrow 2[AlO_2]^-(sol)$.

Thus, by changing the pH_2O, we can control the solubility of a metal oxide in acidic or basic conditions. Since there is no single, unique set of conditions to achieve a specific pH_2O (MOH, temperature, water), we have much experimental freedom to carry out these reactions.

When thinking about the chemistry occurring in molten hydroxides, we must consider additional chemical processes having to do with the presence of oxygen in the melt. Molten hydroxides support the presence of peroxides and superoxides; species that can oxidize dissolved metals and thereby affect their solubilities [30].

Peroxides are believed to form according to

$$O_2(sol) + 4OH^-(l) \rightleftarrows 2O_2{}^{2-}(sol) + 2H_2O(sol) \quad (5)$$

while superoxides are believed to form in hydroxide melts by the following process:

$$3O_2(sol) + 4OH^-(l) \rightleftarrows 4O_2{}^{-}(sol) + 2H_2O(sol) \quad (6)$$

The stabilization of dissolved peroxides and superoxides in hydroxide fluxes follows the trend found for the alkali metal oxides to stabilize peroxide and superoxides in the solid state. Thus, lithium hydroxide provides a negligible stabilization of peroxides or superoxides; sodium hydroxide stabilizes the peroxide species, while potassium, rubidium and cesium hydroxides stabilize both peroxides and superoxide species. The oxidizing potential of the hydroxide melts, consequently, increases down the group of alkali metals, with cesium hydroxide supporting the most oxidizing conditions.

We can use all this information for planning reactions to grow crystals of complex oxides out of hydroxide melts, although a significant amount of additional information will have to be determined experimentally. For example, the solubilities of most metals in molten hydroxides have not been determined, making it necessary to perform exploratory studies to establish the conditions (temperature, MOH, pH_2O) under which and to what extent they are soluble. Clearly, the pH_2O is one of the most important parameters that needs to be controlled, and that means controlling the water content of the melt during the crystal growth process. At low temperatures, 200–400 °C, water loss via evaporation is "slow" and thus open crucibles can be used to maintain acidic conditions for several hours. Longer reactions times, however, will result in loss of water via evaporation and a change of the melt from acidic to basic. At times, this may be desirable, as the increase in pH_2O will reduce the solubility of many metals and, thereby, induce crystal growth. In order to operate at higher temperatures, however, closed systems must be used if one wants to avoid rapid evaporative water loss and the resulting basic conditions. In the extreme case, the hydroxide melt will transform into a highly basic molten oxide via

$$2MOH(l) \rightleftarrows H_2O(g) + M_2O(l) \quad (7)$$

This, of course, may be desirable in many instances and a large number of oxides have been prepared starting with the basic anhydride oxides [31–66].

3. Methods

In this section, detailed descriptions of experimental considerations, such as reaction vessel, temperature, and time and the experimental procedure are presented. A schematic of the relevant variables is provided in Fig. 2. Typical starting reagents for hydroxide flux reactions are lanthanide sesquioxides (Ln_2O_3), platinum group metals (Ru, Os, Ir, Rh, Pd, Pt), platinum group metal oxides (RuO_2) or salts ($(NH_4)_2PtCl_6$), and alkali metal hydroxides (MOH). The choice and reactivity of hydroxide, reaction vessel, and reaction parameters such as temperature and time are important variables that contribute considerably to the final outcome of a reaction. The choice of hydroxide depends on the desired reactivity of the hydroxide. A flux can be either "reactive", meaning the alkali metal from the hydroxide is incorporated into the product, or "un-reactive", meaning the hydroxide acts purely as a solvent of crystallization and the alkali metal is not incorporated into the product.

The vessels utilized to contain a reaction include, but are not limited to, silver crucibles, alumina crucibles, and silver tubes and are selected based on the desired reaction environment. Silver

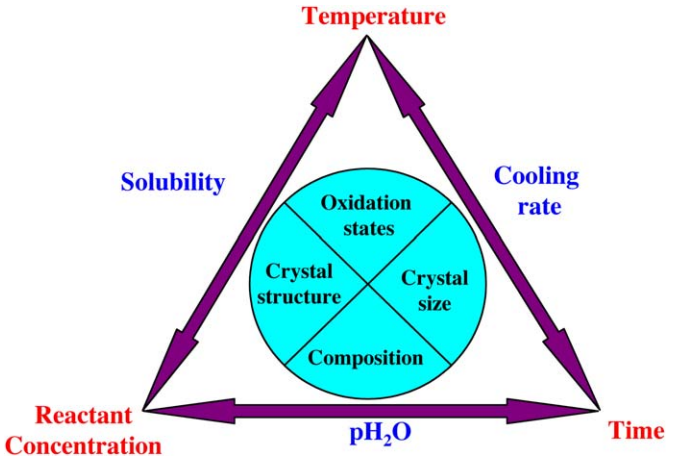

Fig. 2. Schematic of the relevant experimental variables influencing the formation of single crystals synthesized using the hydroxide flux method.

tubes, silver crucibles and alumina crucibles affect hydroxide reactions very differently in that alumina is slightly soluble in molten hydroxide while silver is sparingly soluble, if at all. More importantly, since alkali metal hydroxides typically contain 15–20% water right out of the bottle and adding water to a reaction increases the acidity, the choice to use an open reaction vessel (crucible) as opposed to a closed reaction vessel (tube) greatly affects the acid–base properties of the melt and can influence the product of a reaction as previously discussed. The water content can also be controlled by the heating rate, dwell time and cooling rate as determined in the reaction profile.

3.1. Silver tubes

The use of sealed silver tubes offers a unique advantage over crucibles in that the tubes can be sealed to avoid water loss via evaporation at elevated temperatures. Silver melts at 962 °C, permitting operation to near 900 °C, before softening of the tube leads to loss of structural integrity due to the mild, but noticeable vapor pressure in the tube. (In a hydroxide melt, unlike in a hydrothermal reaction where water becomes supercritical at temperatures exceeding 374 °C with a pressure of 218 atmospheres, water is solvated and, thus, the flux generates only a very minor vapor pressure.) Furthermore, silver does not react with the hydroxide flux [67,68], and is considered an inert reaction vessel with respect to hydroxides. Finally, silver supports oxygen diffusion at elevated temperatures [69,70], enabling some gas exchange between the melt and the atmosphere surrounding the silver tube. The atmosphere over the molten hydroxide will affect the presence of peroxide and superoxide species in the melt and thus alter the redox equilibria that control the stability of metal oxidation states in the melt.

Practical silver tubes are 1 cm in diameter and after being cut into smaller pieces are approximately 10 cm long. One end of a tube is crimped shut and flame sealed. The starting reagents (0.25–1 mmol for non-flux reagents) are loaded into the open end of the tube with the flux added last. The amount of flux added depends on the physical shape of the flux. For example, if the alkali metal hydroxide is in pellet form, 3–4 g of flux fill a tube and still allow room at the top to close the tube. After the reactants have been loaded into the tube, the open end is crimped shut and folded over three times. The folded end is then hammered or spot welded shut to ensure that no leaking will occur. The tube is placed upright in a programmable box furnace with the flame sealed end at the bottom.

3.2. Crucibles

Open silver and alumina crucibles are utilized when control of the reaction environment is not essential or if a drier, more basic, flux is desired. The starting reagents depend upon the desired composition where typically 0.25–1 mmol of each non-flux reagent and 10–30 g of alkali metal hydroxide are utilized. The non-flux reagents are charged into the crucible and are covered by the hydroxide. Both forms of crucibles can be covered with lids and typically are placed into a programmable furnace for heating.

3.3. Reaction profile

The temperature and time affect the outcome of a hydroxide reaction with heating and cooling rates, as well as the dwell temperature and time influencing the formation of kinetically and thermodynamically favored products. Dwell temperatures can range from the melting point of the hydroxide to slightly less than the melting point of the reaction vessel, but typically range from 500 to 800 °C. Crystal growth is highly temperature dependent where, upon changing the reaction temperature by as little as 50 °C, we observe crystal formation in a system that did not yield a desired product at the initial temperature. Interestingly, at different temperatures, the same system of reagents can yield surprisingly different phases and structures as will be discussed in detail later in this review. The total reaction time is dictated by the heating rate, the dwell time, and the cooling rate. The heating rate is usually fairly rapid at 10 °C/min, but slower rates can be used to slow the loss of water. The dwell time ranges from 5 to 72 h, but most commonly 12–24 h dwell times are utilized. In some systems, crystal quality and size are affected by the dwell time and cooling rate. The rate of cooling is usually determined by shutting off the furnace after the dwell time has completed and allowing the reaction to cool to room temperature. However, slow cooling at 1–10 °C/h can result in crystals of higher quality and/or larger size.

The synthetic flexibility available in molten hydroxide flux growth has lead to an abundance of new structures and compositions and allows for many different systems to be explored. The results we have obtained from our exploration of platinum group (Ru, Os, Ir, Rh, Pd, Pt) and lanthanide metals in molten alkali metal hydroxides will be detailed below with emphasis placed on structural and compositional trends as influenced by the size and coordination environment of the constituent lanthanide metals.

4. Discussion of results

For more than a decade the zur Loye group has focused on the discovery of new platinum group metal oxide materials through crystal growth from high temperature solutions. Our initial efforts in the crystal growth of platinum group metal oxides utilized alkaline earth carbonates as a solvent of crystallization for the successful preparation of several new oxides of Rh, Pt, Ir, and Ru [2,71–73]. Subsequently, we began work using molten hydroxides as a solvent from which we could prepare single crystals of complex oxides of the platinum group metals due to the flux's ability to effectively dissolve reagent species of interest. These efforts yielded considerable success in isolating complex oxides of the platinum group. Typically, these reactions were carried out using an alkaline earth metal as the large electropositive cation, and as a result many perovskite-related phases were prepared. Examples include: 6H-perovskites $Ba_3MM'_2O_9$ (M = Li, Na, M' = Ru [74], Os [75], Ir [76]), 2H-perovskites exemplified by Sr_3LiRuO_6 [72], an oxygen deficient 7L-perovskite $Ba_7Li_3Ru_4O_{20}$ [77], the 8H-perovskite $Ba_4Na_3Ru_4O_{12}$ [77], and the double perovskites Ba_2MOsO_6 (M = Li, Na) [78]. Many other platinum group metal oxides have been prepared by different methods or by using fluxes other than molten hydroxides and, consequently, will not be discussed in this brief overview. Therefore, the reader is directed to the very extensive work by Hoppe and Müller-Buschbaum, only a small portion of which is referenced here [31–66].

As a natural progression, it became desirable to investigate the crystal growth of lanthanide metal containing oxides of the platinum group, and molten hydroxides were selected as an appropriate solvent. It has been shown that molten hydroxides are capable of dissolving the metals of the lanthanide series [14,16], where the solubility of the lanthanides is dictated by the acid–base properties of the melt. Specifically, the water content of the melt must be controlled to enable the dissolution of the lanthanide oxides (Ln_2O_3's) [25–27], which are more soluble in acidic "wet" melts [16]. We have found that as a function of the size of the lanthanide cation, Ln^{3+}, different structure types are

isolated within the confines of reaction with a particular platinum group metal.

4.1. Oxides of ruthenium, osmium, and iridium

There have been many research efforts directed at the synthesis and characterization of ruthenates and iridates, where most studies utilized traditional solid-state powder techniques to prepare new compositions of known structure types. Osmates have been somewhat neglected until recently when interest in complex osmates increased, in part, because of the superconducting properties of AOs_2O_6 (A = K, Rb) [79,80]. Our research efforts employing molten hydroxides have resulted in the synthesis of many new complex ruthenates, iridates, and osmates of both known and novel structure types. Based on their similar sizes, octahedral coordination environment preference, and their ability to accommodate a wide range of oxidation states, iridium, ruthenium and osmium can often be substituted for one another in many different structure types making them ideal for studying structure property relationships. The compositional flexibility that exists in the first two structure types discussed below, the double perovskites, $Ln_2MM'O_6$ (Ln = La, Pr, Nd, Sm, Eu; M = Li, Na; M' = Ru, Ir, Os) [81–86] and the defect fluorites, Ln_3MO_7 (Ln = Pr, Nd, Sm, Eu, Gd; M = Ru, Ir, Os) exemplifies the structural similarities and chemical differences among these platinum group metals.

4.1.1. Double perovskites $Ln_2MM'O_6$

The double perovskites of the general formula $Ln_2MM'O_6$ [81–86], where M is either Li^+ or Na^+, thus requiring that M' be a pentavalent metal, were isolated from reactive hydroxide fluxes. These reactions were carried out in sealed silver tubes at temperatures at or between 600 and 700 °C for times ranging from 12 to 72 h. Such reactions yielded single crystals of all phases with similar morphologies.

All of these compounds crystallize in the space group $P2_1/n$, with the monoclinic distorted double perovskite structure type, Fig. 3. In these compounds, the M^+ and M'^{5+} cations reside on the octahedral sites while the Ln^{3+} cations occupy the A site in an eight-fold coordination environment. This space group allows for the 1:1 ordered arrangement of the M and M' cations in a rock-salt type lattice, and also takes into account the tilting of the MO_6 and $M'O_6$ octahedra necessary to accommodate the small size of the Ln^{3+} cation. This structure persists for larger cations of the lanthanide series and seems to be a function of the Goldschmidt tolerance factor (t) [8]. As t decreases, the perovskite structure becomes less likely to be stable and lower limits for t appear to be around 0.86 [87], which is consistent with our experimental findings, Table 2.

4.1.2. Defect-fluorite oxides Ln_3MO_7

The defect-fluorite oxides, Ln_3MO_7 (Ln = Pr, Nd, Sm–Gd, M = Ir, Ru, Os) [88–91] were isolated as single crystals from hydroxide flux reactions carried out in sealed silver tubes at 600–700 °C for times ranging from 12 to 24 h. The family of compounds with the general formula Ln_3MO_7, where Ln is a lanthanide and M is a pentavalent transition metal cation, were first reported by Allpress and Rossell in 1979 and were described as having an orthorhombic, fluorite-related structure [92]. The structure of these compounds is well described in the orthorhombic space group $Cmcm$ and features chains of trans vertex-sharing MO_6 octahedra that are oriented along the c-axis and that are tilted in the bc plane [93]. In this structure, the lanthanide cations are located in two different coordination environments, eight-fold pseudo-cubic and seven-fold pentagonal bipyramidal, and the M(V) cations are located in octahedral coordination, Fig. 4(a).

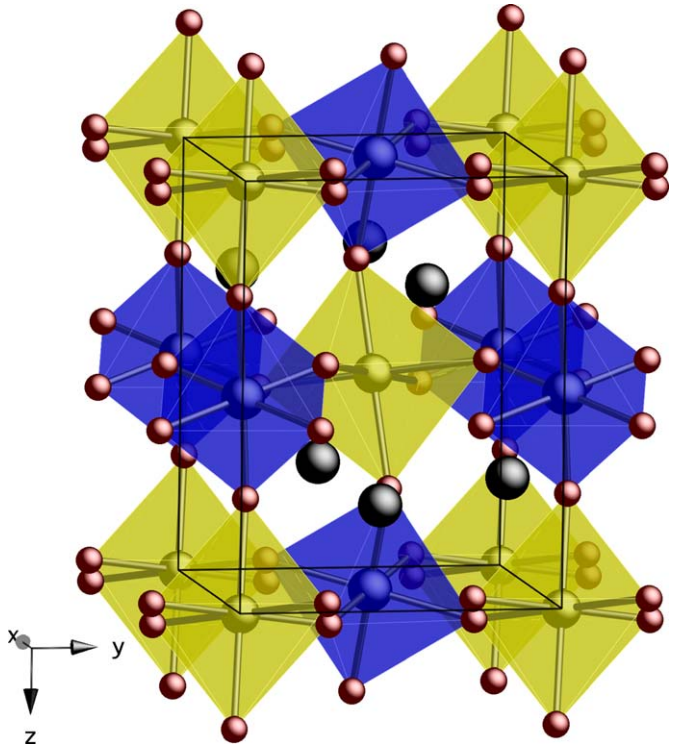

Fig. 3. Crystal structure of the monoclinically distorted double perovskites with the general formula $Ln_2M^+M^{5+'}O_6$ (Ln = La, Pr, Nd, Sm, Eu; M^+ = Li, Na; $M^{5+'}$ = Ru, Os, Ir). MO_6 octahedra are shown in yellow, $M'O_6$ octahedra in blue, lanthanide atoms are black spheres, and oxygen atoms are red spheres. (For interpretation of the references to color in this figure legend, the reader is referred to the web version of this article.)

Table 2
Goldschmidt tolerance factor (t) and magnetic properties of the lanthanide containing double perovskites, $Ln_2MM'O_6$ (Ln = La, Pr, Nd, Sm, Eu; M = Li, Na; M' = Ir, Ru, Os), synthesized in this study.

Double perovskite	t	Magnetism
La_2LiIrO_6	0.94	PM
Pr_2LiIrO_6	0.93	PM
Nd_2LiIrO_6	0.92	PM
Sm_2LiIrO_6	0.91	PM
Eu_2LiIrO_6	0.90	PM
La_2NaIrO_6	0.89	PM
Pr_2NaIrO_6	0.88	PM
Nd_2NaIrO_6	0.86	PM
Sm_2NaIrO_6	0.85	N
La_2LiOsO_6	0.93	AFM, $T_N = 39$ K
Pr_2LiOsO_6	0.92	AFM, $T_N = 35$ K
Nd_2LiOsO_6	0.91	AFM, $T_N = 23$ K
Sm_2LiOsO_6	0.90	AFM, $T_N = 32$ K
La_2NaOsO_6	0.89	AFM, $T_N = 16$ K
Pr_2NaOsO_6	0.88	CAFM, $T < 10$ K
Nd_2NaOsO_6	0.86	AFM1, $T_{N1} = 20$ K AFM2, $T_{N2} = 10$ K FM, $T < 20$ K, field > 20 kG
La_2NaRuO_6	0.89	AFM, $T_N = 16$ K
Pr_2NaRuO_6	0.88	CAFM, $T < 20$ K
Nd_2NaRuO_6	0.87	CAFM, $T < 18$ K

In the table PM = paramagnetic, AFM = antiferromagnetic, FM = ferromagnetic, CAFM = canted antiferromagnetic, and N = magnetic studies were not performed. The temperature at which magnetic ordering is observed is also listed.

Interestingly, detailed magnetic and thermal investigations were reported for the ruthenium and iridium containing members

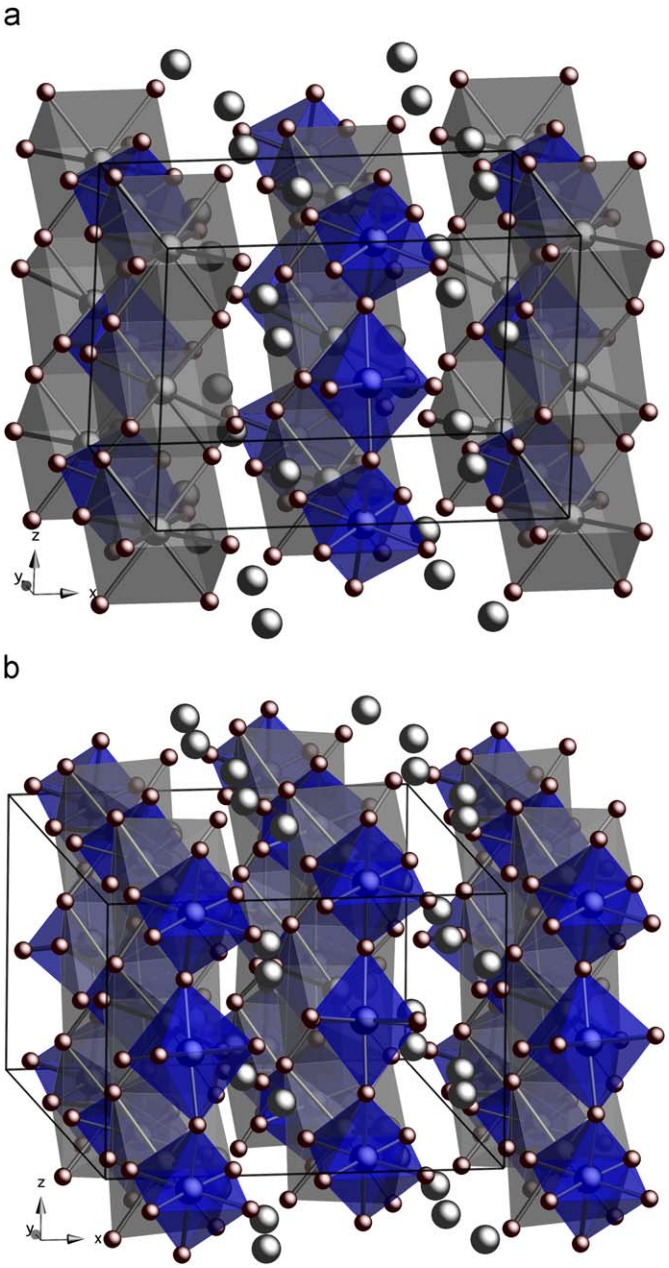

Fig. 4. (a) Drawing of the *Cmcm* crystal structure of the Ln_3MO_7 (*Ln* = La, Pr, Nd, Sm–Gd; *M* = Ru, Os, Ir) fluorite-related phases emphasizing the chains of trans vertex-sharing MO_6 octahedra (blue) that are edge-shared to the chains of $Ln(1)O_8$ pseudo-cubes (gray) along the *c*-axis. The gray spheres are the $Ln(2)^{3+}$ cations. (b) Drawing of the low temperature $P2_1nb$ structure of the Ln_3MO_7 phases emphasizing the chains of trans vertex-sharing MO_6 octahedra (blue) that are edge shared to chains of $Ln(1,2)O_7$ mono-capped trigonal prisms (gray) along the *c*-axis. The gray spheres are the $Ln(3–6)^{3+}$ cations. (For interpretation of the references to color in this figure legend, the reader is referred to the web version of this article.)

Table 3
Magnetic properties of the lanthanide containing fluorite related oxides, Ln_3MO_7 (*Ln* = Pr, Nd, Sm–Gd; *M* = Ir, Ru, Os), synthesized in this study.

Ln_3MO_7	Magnetism
Pr_3IrO_7[a]	PM
Nd_3IrO_7[a]	AFM, $T_N = 2.6$ K
Sm_3IrO_7[a]	PM
Eu_3IrO_7[a]	PM
Sm_3RuO_7	AFM, $T_N = 6$ K
Eu_3RuO_7	AFM, $T_N = 18$ K
Sm_3OsO_7	AFM, $T_N = 35$ K
Eu_3OsO_7	AFM, $T_N = 23$ K
Gd_3OsO_7	AFM, $T_N = 34$ K

In the table, PM = paramagnetic, AFM = antiferromagnetic, and FM = ferromagnetic. The temperature at which magnetic ordering is observed is also listed.
[a] Magnetic properties previously reported [94–98,157].

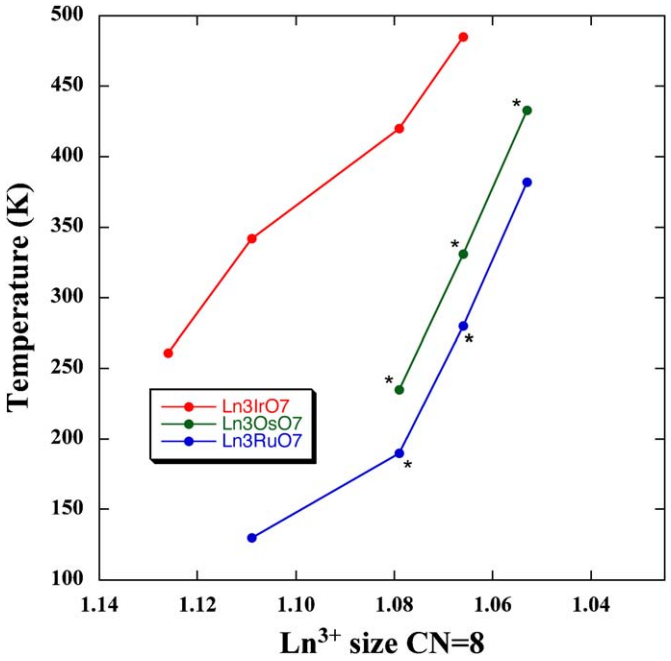

Fig. 5. Transition temperatures for the compounds of the stoichiometry Ln_3MO_7 (*M* = Ir, Os, Ru). Compositions investigated by us are marked by an asterisk. Above the marker, the compound exists in the high-temperature *Cmcm* form, and below the marker the compound exists in the low-temperature $P2_1nb$ structure.

of the Ln_3MO_7 family (Table 3), which provided evidence for the existence of low temperature structural phase transitions and that showed that the transition temperature is a function of the specific lanthanide ion in the Ln_3MO_7 (*M* = Ir, Ru) oxides [94–98]. The use of molten hydroxides as a solvent yielded high quality single crystals of Ln_3MO_7 (*Ln* = Sm, Eu, Gd, *M* = Ru, Os) and we subsequently described the observed structural phase transition from space group *Cmcm* to $P2_1nb$ [88,89] (Fig. 4(b)). The structure transition results in a distortion of the vertex-shared Ru–O chains, and a reduction in the coordination of one of the rare earth cations from eight- to seven-fold in addition to a loss of lattice centering and doubling of the *b*-axis, Fig. 5.

When the compositional flexibility in structures is limited because of cation size, coordination environment, or oxidation state constraints, iridates, ruthenates, and osmates can form structure types specific to only one particular platinum group metal. The size of the lanthanide and/or alkali metal as well as the reaction conditions (temperature, vessel, acidity/basicity) are perhaps the two most important factors that contribute to the stabilization of a particular composition or structure type prepared from hydroxide flux reactions. As the size of the constituent alkali metal increases or the size of the constituent lanthanide decreases the double perovskite structure and the fluorite-related structures are no longer stable. Therefore, synthetic efforts utilizing molten hydroxides often yield new and complex structure types if the difference in the cation sizes becomes too great. The utility of hydroxide flux reactions as a unique approach for discovering new complex structure types will be exemplified in the structural investigations in the paragraphs that follow.

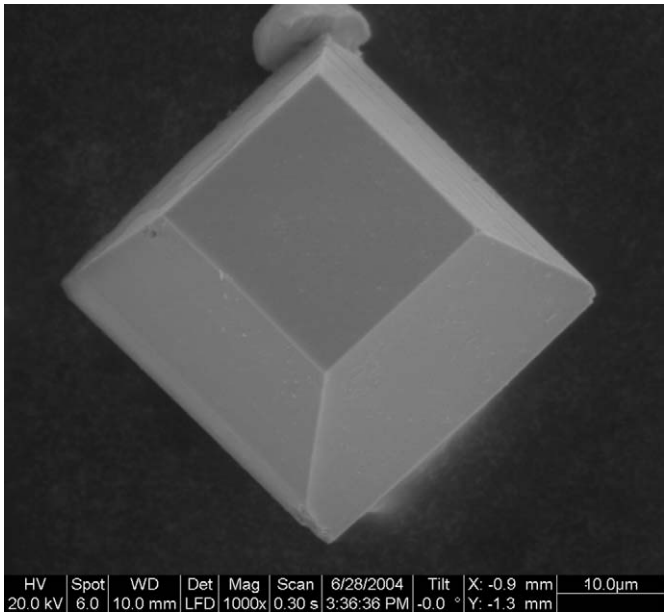

Fig. 6. Scanning electron micrograph of a single crystal of $Tb_5Ru_2O_{12}$.

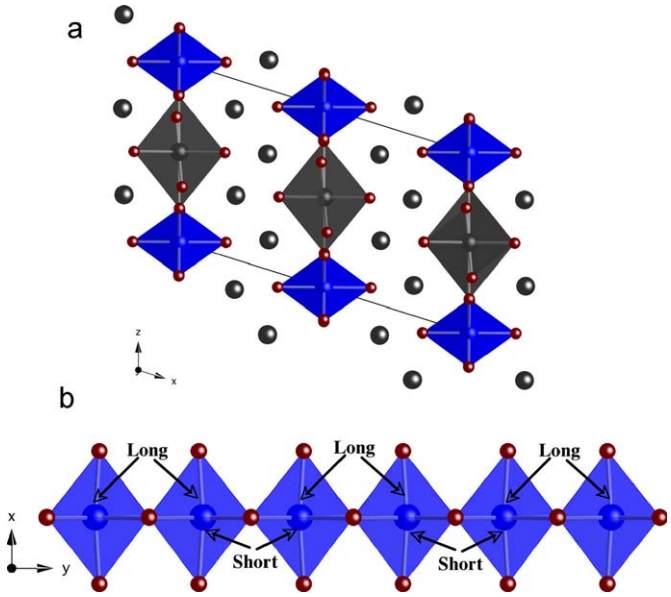

Fig. 7. (a) Crystal structure of $Eu_5Ru_2O_{12}$, which is representative of the series $Ln_5Ru_2O_{12}$ (Ln = Nd, Sm–Tb). RuO_6 octahedra are blue, Eu(3)O_6 octahedra are gray, Eu(1) and Eu(2) are represented by gray spheres, while red spheres represent oxygen atoms. (b) The infinite chains of edge sharing RuO_6 octahedra emphasizing the alternating short (2.780 Å) and long (3.091 Å) Ru to Ru distances in $Eu_5Ru_2O_{12}$. (For interpretation of the references to color in this figure legend, the reader is referred to the web version of this article.)

4.1.3. $Ln_5Ru_2O_{12}$ *[99]*

The rare earth ruthenates $Ln_5Ru_2O_{12}$ (Ln = Nd–Tb) were isolated as single crystals from either sodium or potassium hydroxide flux reactions carried out in sealed silver tubes at 600 °C for 12–24 h, Fig. 6. The structure of these compounds features edge sharing MO_6 octahedra forming infinite chains that are separated by rare earth cations, Fig. 7(a). Within the chains of edge sharing MO_6 octahedra, the metal-to-metal distances alternate between short and long, Fig. 7(b). The average valence state of the metal cations is +4.5. There are relatively few phases

Table 4
Magnetic properties of the remaining lanthanide-containing ruthenates and iridates synthesized during this study.

Compound	Magnetism
$Nd_5Ru_2O_{12}$	AFM, $T_N < 10$ K
$Sm_5Ru_2O_{12}$	AFM, $T_N < 10$ K
$Eu_5Ru_2O_{12}$	AFM, $T_N < 10$ K
$Gd_5Ru_2O_{12}$	AFM, $T_N < 10$ K
$Tb_5Ru_2O_{12}$	CAFM, $T < 10$ K
$Pr_{14}Na_3Ru_6O_{36}$	CAFM, $T < 8$ K
$Nd_{14}Na_3Ru_6O_{36}$	CAFM, $T < 3$ K
$La_{2.5}K_{1.5}IrO_7$	PM
$La_9RbIr_4O_{24}$	PM
$Gd_{0.96}Na_{1.04}IrO_4$	AFM, $T_N = 9$ K
$Tb_{0.93}Na_{1.07}IrO_4$	AFM, $T_N < 2$ K
$Dy_{0.94}Na_{1.06}IrO_4$	AFM, $T_N = 14$ K
$Ho_{0.90}Na_{1.10}IrO_4$	AFM, $T_N = 7$ K
$Er_{0.75}Na_{1.25}IrO_4$	AFM, $T_N = 5$ K
$Y_{0.92}Na_{1.08}IrO_4$	AFM1, $T_{N1} = 33$ K AFM2, $T_{N2} = 10$ K
$Nd_2K_2IrO_7$	PM
$Sm_2K_2IrO_7$	N

In the table, PM = paramagnetic, AFM = antiferromagnetic, CAFM = canted antiferromagnetic, and N = magnetic studies were not performed. The temperature at which magnetic ordering is observed is also listed.

that have been reported to crystallize within this structure type, and some examples include the composition $Y_5Re_2O_{12}$ [100] and $Ln_5Mo_2O_{12}$ [101] (Ln = Y and Gd). All of the compounds exhibit antiferromagnetic behavior at low temperatures and $Tb_5Ru_2O_{12}$ shows evidence of canting at temperatures below 10 K (Table 4).

4.1.4. $Ln_{14}Na_3Ru_6O_{36}$

The hexagonal ruthenates $Ln_{14}Na_3Ru_6O_{36}$ (Ln = Pr, Nd) [102] were isolated as single crystals from sodium hydroxide flux reactions carried out in sealed silver tubes at 600 °C for 12 h. The structure is composed of two types of slabs, $Ln(1)_6[Na(2)Ln(3)]_2Na(1)Ru(1)_3O_{18}$ and $Ln(2)_6Ru(2)Ru(3)_2O_{18}$, that alternate in an *AB* fashion. These slabs, consisting of three layers each, are propagated via a 3_1 screw axis to yield a unit cell with a 12-layer structure. The complete structure of $Nd_{14}Na_3Ru_6O_{36}$ is shown in Fig. 8, which is very similar to that of $La_7Ru_3O_{18}$ [103]. All three compounds share virtually the same arrangement of lanthanide, ruthenium, and oxygen atoms. The difference is that in $Ln_{14}Na_3Ru_6O_{36}$ (Ln = Pr, Nd), sodium is present, occupying coordination sites that are vacant in the structure of $La_7Ru_3O_{18}$. Both of these compounds show magnetic behavior that is consistent with canted antiferromagnetism (Table 4).

4.1.5. $La_{2.5}K_{1.5}IrO_7$ *and* $La_9RbIr_4O_{24}$

As demonstrated in the double perovskite series, lithium and sodium hydroxide can be utilized as reactive fluxes and their ionic radii in an octahedral coordination environment (Li = 0.76 Å; Na = 1.02 Å) [7] make them suitable *B*-site cations in the double perovskite structure. Alkali metals with greater ionic radii, such as potassium (1.38 Å) [7] or rubidium (1.52 Å) [7] are too large to occupy the *B*-site of the double perovskite structure; thus, synthetic exploration utilizing potassium and rubidium hydroxide fluxes led to the isolation of the perovskite-related oxides, $La_{2.5}K_{1.5}IrO_7$ [104] and $La_9RbIr_4O_{24}$ [105]. The reactions were carried out in sealed silver tubes or covered silver crucibles at 650 °C over a period of 24 h. The $La_{2.5}K_{1.5}IrO_7$ crystals were black and hexagon-shaped, while the $La_9RbIr_4O_{24}$ crystals were black and rectangular block-shaped.

$La_{2.5}K_{1.5}IrO_7$ is an $n = 2$ member of the $[A_nB_{n-1}O_{3n}][A'_2O]$ family of oxides consisting of close-packed $[AO_3]$ and $[A'_2O]$ layers [106–116]. A representation of the crystal structure is shown in

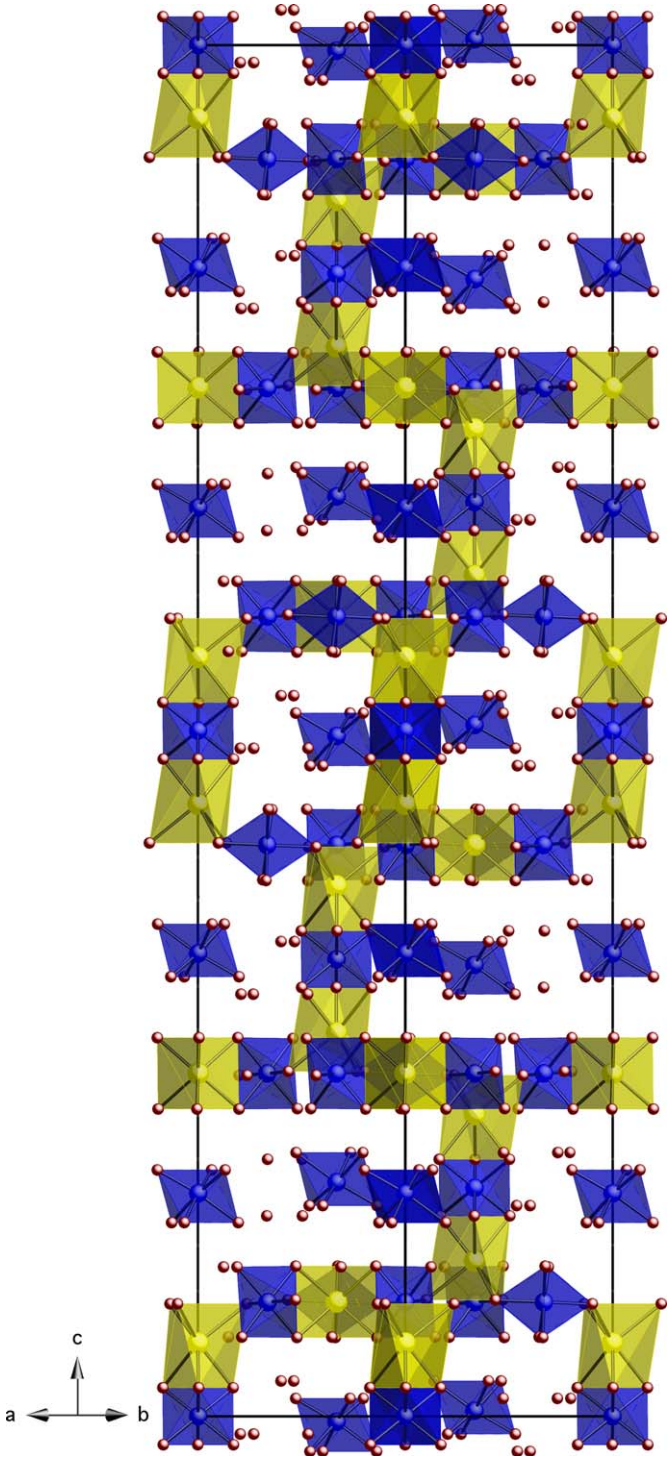

Fig. 8. The crystal structure of the ruthenates with general formula $Ln_{14}Na_3Ru_6O_{36}$ (Ln = Pr, Nd). NaO_6 polyhedra are shown in yellow, RuO_6 octahedra are shown in blue, oxygen atoms in red and the Nd^{3+} atoms have been omitted for clarity. (For interpretation of the references to color in this figure legend, the reader is referred to the web version of this article.)

Fig. 9 with the crystal structure of $Ba_{3.44}K_{1.56}Ir_2O_{10}$, an $n = 3$ member of this family also grown from a molten hydroxide flux [76], shown to the right for comparison. The structure consists of anionic $[La_2IrO_6]^-$ layers that contain lanthanum atoms in a seven-fold coordination environment and isolated IrO_6 octahedra. These layers are charge compensated by cationic $[La_{0.5}K_{1.5}O]^+$ layers that contain mixed occupancy lanthanum/potassium

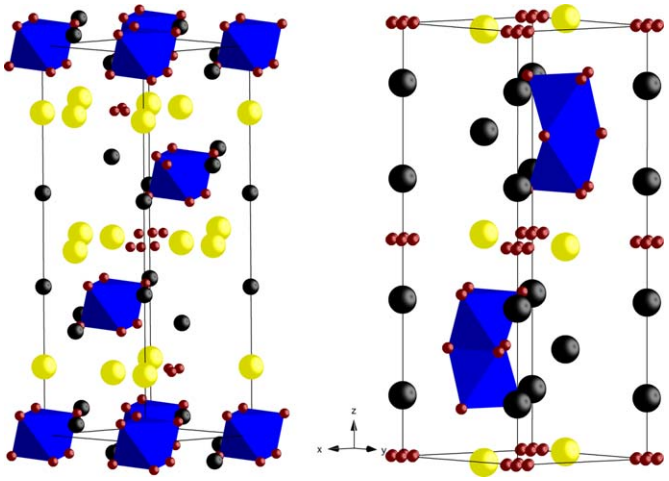

Fig. 9. The crystal structures of $n = 2$ member, $La_{2.5}K_{1.5}IrO_7$ (left) and $n = 3$ member, $Ba_{3.44}K_{1.56}Ir_2O_{10}$ (right) of $[A_nB_{n-1}O_{3n}][A'_2O]$ family of oxides. In the $La_{2.5}K_{1.5}IrO_7$ structure, the IrO_6 octahedra are blue, La(1) atoms are black spheres, La(2)/K(2) atoms are yellow spheres, and the oxygen atoms are red spheres. In $Ba_{3.44}K_{1.56}Ir_2O_{10}$, the Ir_2O_9 face-shared octahedra dimers are blue, the barium atoms are black spheres, the Ba(3)/K(1) atoms are yellow spheres, and the oxygen atoms are red spheres. (For interpretation of the references to color in this figure legend, the reader is referred to the web version of this article.)

capped trigonal prismatic sites to yield an overall charge neutral structure. There was no evidence of magnetic ordering observed in the magnetic susceptibility data of $La_{2.5}K_{1.5}IrO_7$ (Table 4).

$La_9RbIr_4O_{24}$ represents a rare rubidium containing oxide that crystallizes in a new structure-type. A polyhedral representation of the structure is shown in Fig. 10 and can be described as arising from the $ABA'BA$ stacking of two different slabs: $LaRbIr_2O_{10}$ (A), and $La_8Ir_2O_{14}$ (B), where the A' layer is offset by $(\frac{1}{2}x, \frac{1}{2}y, \frac{1}{2}z)$ from the A layer. The A layer consists of a large, RbO_{14} octa face-capped octahedron that vertex-shares to four LaO_6 octahedra at the corners of the cell and face-shares to four IrO_6 octahedra situated on the edges of the unit cell. In addition, the IrO_6 octahedra corner-share with the LaO_6 octahedra. The B layer contains five isolated IrO_6 octahedra, four of which are located on the edges of the unit cell, while the fifth octahedron is located at the center, directly below the rubidium atom of the A layer. The large size of the rubidium atom forces this central IrO_6 octahedron slightly out of the plane that contains the other isolated IrO_6 octahedra. The space in the $La_8Ir_2O_{14}$ slabs that is not occupied by the IrO_6 octahedra is filled by the lanthanum cations that are located in distorted, capped-trigonal prismatic environments. The layers are all connected via chains of LaO_6–IrO_6–RbO_{14}–IrO_6–LaO_6 corner-shared polyhedra that run along the c-direction. There was no evidence of magnetic ordering observed in the magnetic susceptibility data of $La_9RbIr_4O_{24}$ (Table 4).

4.1.6. $Ln_{1-x}Na_{1+x}IrO_4$ (Ln = Gd–Er, Y; $x = 0.04$–0.25)

As demonstrated in the preceding compositions, the incorporation of the larger alkali metals, potassium and rubidium, into the La–M–Ir–O (M = alkali metal) reaction system resulted in the crystallization of phases structurally related to the perovskite, but exhibiting distinct novel structure types. Similarly, as one continues across the lanthanide series the decreasing size of the constituent lanthanide no longer allows for the formation of the perovskite structure. A new series of hexagonal iridates, $Ln_{1-x}Na_{1+x}IrO_4$ (Ln = Gd–Er, Y) [117] were grown from mixed sodium/cesium hydroxide flux reactions, where sodium was a reactive component in the flux and was incorporated into the structure because it is of similar size to the constituent

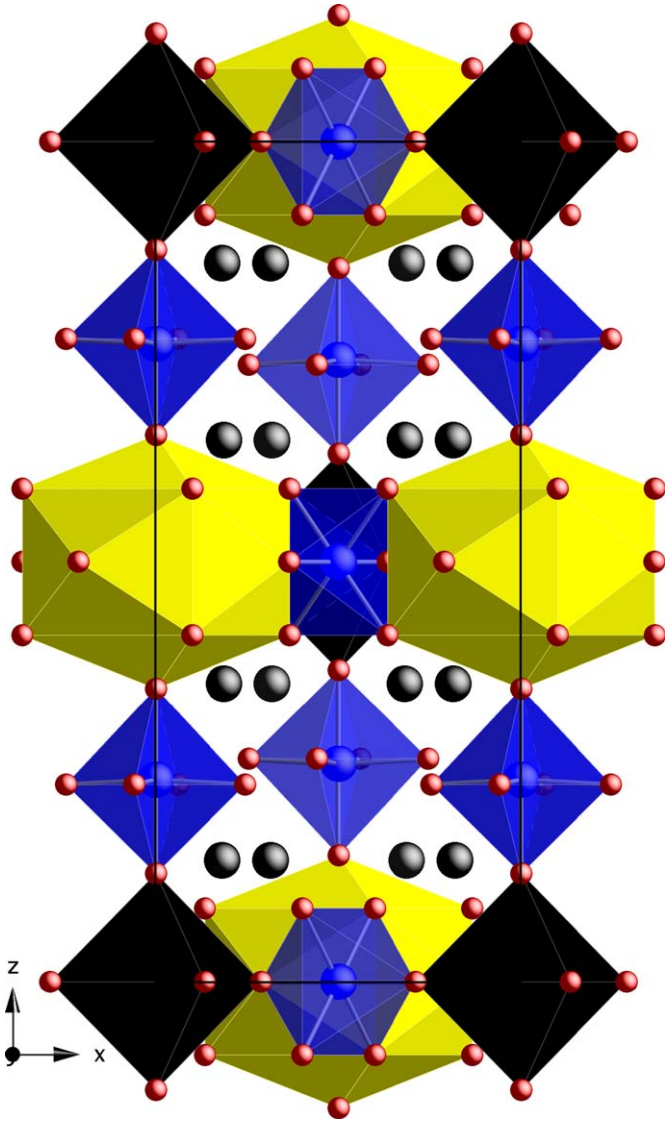

Fig. 10. The crystal structure of $La_9RbIr_4O_{24}$ viewed along the [010] (*b* axis). RbO_{14} polyhedra are shown in yellow, IrO_6 octahedra in blue, and LaO_6 octahedra in black. Lanthanum and oxygen atoms are black and red spheres, respectively. (For interpretation of the references to color in this figure legend, the reader is referred to the web version of this article.)

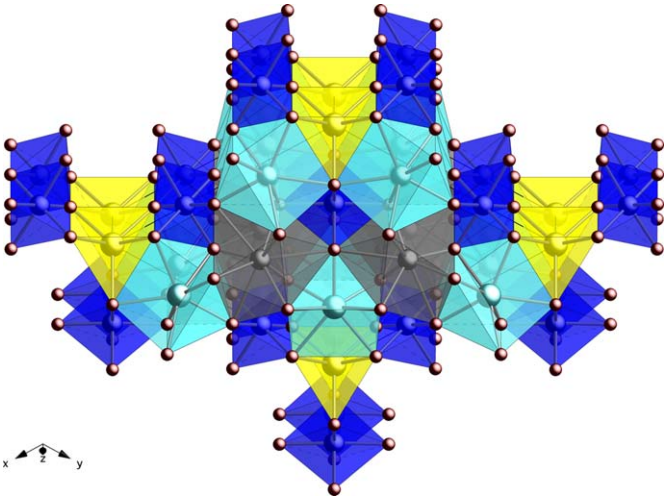

Fig. 11. Crystal structure of the $Ln_{1-x}Na_{1+x}IrO_4$ (Ln = Gd–Er, Y) viewed along the *z*-direction. NaO_6 trigonal prisms are shown in yellow, IrO_6 octahedra in dark blue, $Ln(2)$/Na(2) capped-trigonal prisms in light blue, and $Ln(1)O_9$ polyhedra in gray. Oxygen atoms are represented as red spheres. (For interpretation of the references to color in this figure legend, the reader is referred to the web version of this article.)

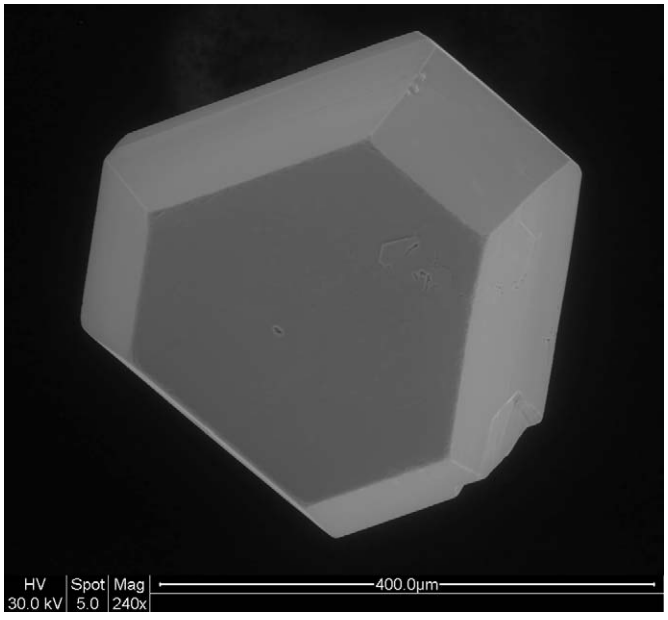

Fig. 12. A scanning electron micrograph of a single crystal of $Nd_2K_2IrO_7$.

lanthanides. The reactions were carried out in sealed silver tubes or covered silver crucibles at 650 °C over a period of 24 h.

Single crystals of $Ln_{1-x}Na_{1+x}IrO_4$ (Ln = Gd–Er, Y) formed as black hexagonally capped rods and are structurally related to the $Ca_{2-x}IrO_4$ family of iridates that was first reported many years ago [118–123]. In this series, the $Ca_{2-x}IrO_4$ (A_2BO_4) structure was essentially modified by replacing the two Ca^{2+} cations with one Ln^{3+} and one Na^+ cation, thereby generating the generic formula $AA'BO_4$. Interestingly, as the size of the lanthanide cations decreases from Gd–Er, the composition adjusts itself by substituting sodium onto the lanthanide site to maintain structural stability. As a result, the oxidation state of iridium increases from +4.08 in $Gd_{0.96}Na_{1.04}IrO_4$ to +4.50 in $Er_{0.75}Na_{1.25}IrO_4$. A polyhedral representation of the $Ln_{1-x}Na_{1+x}IrO_4$ (Ln = Gd–Er, Y; x = 0.04–0.25) crystal structure is shown in Fig. 11. The structure consists of a network of edge- and face-shared polyhedra extending infinitely in the *z*-direction with the NaO_6 trigonal prisms anchoring three IrO_6 octahedra at the corners of the unit cell. $Gd_{0.96}Na_{1.04}IrO_4$, $Dy_{0.94}Na_{1.06}IrO_4$, $Ho_{0.90}Na_{1.10}IrO_4$, and $Er_{0.75}Na_{1.25}IrO_4$ exhibit antiferromagnetic correlations below 15 K, whereas in the case of $Tb_{0.93}Na_{1.07}IrO_4$, magnetic correlations do not appear to occur until below 2 K. The magnetic susceptibility data of $Y_{0.92}Na_{1.08}IrO_4$, exhibit the highest magnetic transition temperature of 33 K, with a second magnetic transition around 10 K (Table 4).

4.1.7. $Nd_2K_2IrO_7$ *and* $Sm_2K_2IrO_7$

Oxides containing Ir^{6+} cations are very rare and have previously only been prepared in polycrystalline form using high-pressure synthetic techniques [125–127]. The use of molten hydroxides has led to the first ambient pressure synthesis of all—Ir^{6+} containing oxides, $Ln_2K_2IrO_7$ (Ln = Nd, Sm) [124]. Single crystals of these compounds were obtained from reactive

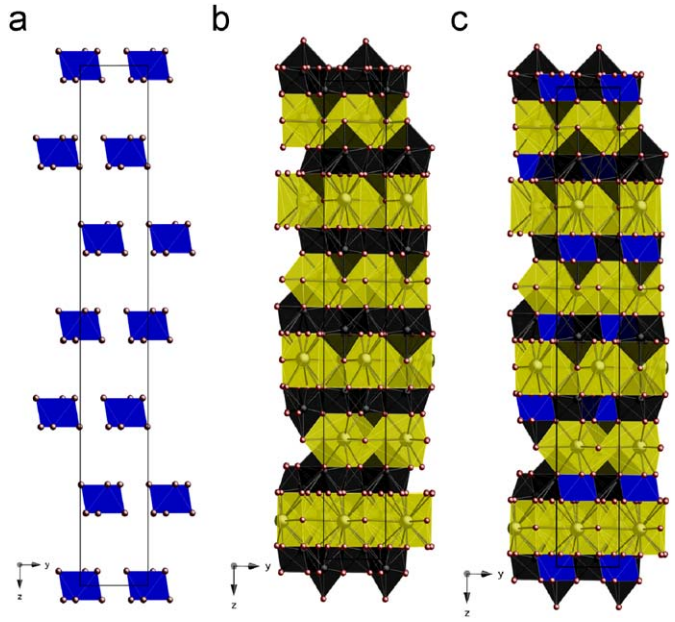

Fig. 13. Crystal structure of $Nd_2K_2IrO_7$ showing: (a) the layers of isolated IrO_6 octahedra (blue), (b) the slabs of KO_{10} polyhedra (yellow) and NdO_{10} polyhedra (black), and (c) the full structure with oxygen atoms shown in red. (For interpretation of the references to color in this figure legend, the reader is referred to the web version of this article.)

potassium hydroxide flux reactions in silver crucibles at 550 °C for 24 h.

Single crystals of $Ln_2K_2IrO_7$ (Ln = Nd, Sm) formed as black, hexagonal plates (Fig. 12). The crystal structure represents a new structure type related to the $[A_nB_{n-1}O_{3n}][A'_2O]$ family of oxides exemplified by $La_{2.5}K_{1.5}IrO_7$ [104] and consists of an intricate slab-like network of isolated IrO_6 octahedra, KO_{10} tetra-capped trigonal prisms, and NdO_{10} irregular polyhedra as shown in Fig. 13. The slabs of IrO_6 octahedra are located perpendicular to the c-axis and are shifted by $(\frac{1}{3}x, \frac{1}{3}y, \frac{1}{3}z)$ from each other. The KO_{10} polyhedra connect the slabs of IrO_6 octahedra and are also shifted along the c-axis by $(\frac{1}{3}x, \frac{1}{3}y, \frac{1}{3}z)$. The NdO_{10} polyhedra occupy the space within the slabs of IrO_6 octahedra and additionally connect the slabs of IrO_6 octahedra and KO_{10} polyhedra. There was no indication of ordering in the magnetic susceptibility data for $Nd_2K_2IrO_7$ and magnetic measurements were not performed for $Sm_2K_2IrO_7$ (Table 4).

4.2. Oxides of palladium

When one examines the platinum group metal oxides literature, there exists a multitude of complex iridates, ruthenates, and platinates, whereas, complex palladium oxides, containing palladium in the +2 to +4 oxidation states, are only sparsely represented. The oxidation state of palladium in these oxides is heavily dependent upon the method of synthesis. For example, divalent palladium compounds such as the ternary alkaline earth palladates Sr_2PdO_3, $SrPd_3O_4$, and $CaPd_3O_4$ [128] and the rare-earth palladates Ln_4PdO_7 (Ln = lanthanide) [129–132] and $La_2Pd_2O_5$ [130–132] have been synthesized using traditional high-temperature solid-state techniques. Although not as common as ternary palladates, a number of quaternary phases are known, for example, the alkaline earth palladate $CaBa_2Pd_3O_6$ [133] and the rare-earth palladates $BaPdLn_2O_5$ (Ln = lanthanide) [134], which were isolated from a $BaCl_2$ flux. When palladates with higher oxidation states are desired, high-pressure techniques have been employed resulting in the synthesis of mixed valent palladates, such as $LnPd_2O_4$ (Ln = lanthanide) [54,55], trivalent palladates, such as the $LaPdO_3$ perovskite [135], and tetravalent palladates, such as the 2-H perovskite related oxides Ca_4PdO_6 and Sr_4PdO_6 [136], the pyrochlores $Ln_2Pd_2O_7$ (Ln = lanthanide) [137], and the inverse spinel Zn_2PdO_4 [138]. Several years ago, we reported the hydroxide flux synthesis and subsequent crystal growth of $SrPd_3O_4$ and $CaPd_3O_4$ [139] and naturally, it was desired to further investigate the reactivity of palladium in molten hydroxides and to incorporate lanthanide metals into the reactions, thereby increasing the structural complexity in the resulting products. The results of this ongoing study of the Ln–M–Pd–O phase space are briefly summarized below.

4.2.1. Ordered A_2PdO_3-type palladates

The ordered lanthanide containing palladates, $LnKPdO_3$ (Ln = La, Pr, Nd, Sm–Gd) and the isostructural copper substituted palladate, $PrK(Cu_{0.14}Pd_{0.86})O_3$ [140] were grown from reactive potassium hydroxide flux reactions in alumina crucibles. The reactions were carried out at 750 °C for 5 h and then cooled over 36 h to 600 °C, at which point the furnace was shut off and allowed to cool to room temperature.

Single crystals of $LnKPdO_3$ (Ln = La, Pr, Nd, Sm–Gd) and $PrK(Cu_{0.14}Pd_{0.86})O_3$ formed as golden brown needles and their crystal structure is related to the A_2MO_3 (A = Ca, Sr, Ba; M = Cu, Pd) [32,128,141–149] alkaline earth metal palladates and cuprates. The crystal structure of $LnKPdO_3$ is shown in Fig. 14. Similar to the $Ln_{1-x}Na_{1+x}IrO_4$ (Ln = Gd–Er, Y) series discussed earlier, this series provides another example of the A-site substitution of one trivalent lanthanide metal and one monovalent alkali metal in place of two divalent alkaline earth metals. The crystal structure contains ordered slabs of LnO_7 and KO_7 capped trigonal prisms arranged in a complex network of face-, edge-, and vertex-shared polyhedra which, in turn, share edges with PdO_4 square planes.

4.2.2. The $A_2Pd_6O_8$-type palladates

The new series of lanthanide containing palladates, $LnNaPd_6O_8$ (Ln = Tb–Lu, Y) [150] were prepared from reactive sodium

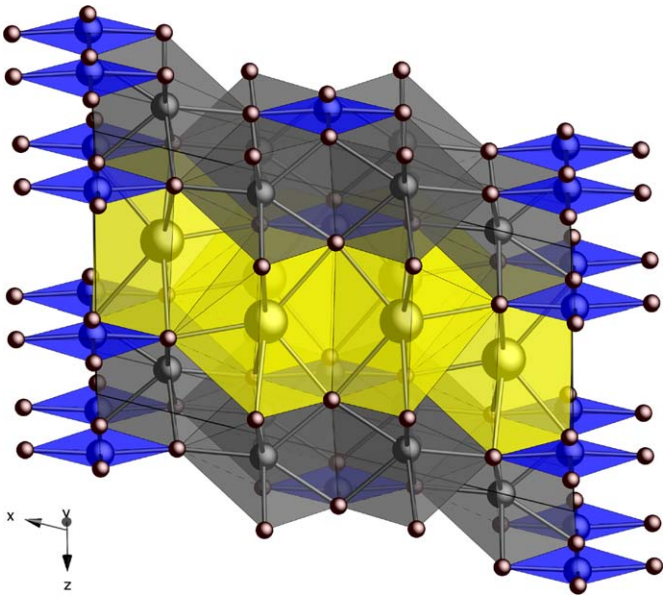

Fig. 14. Crystal structure of the ordered $LnKPdO_3$ (Ln = La, Pr, Nd, Sm, Eu, Gd) palladates. PdO_4 square planes are blue, KO_7 capped trigonal prisms are yellow, LnO_7 capped trigonal prisms are gray, and oxygen atoms are red spheres. (For interpretation of the references to color in this figure legend, the reader is referred to the web version of this article.)

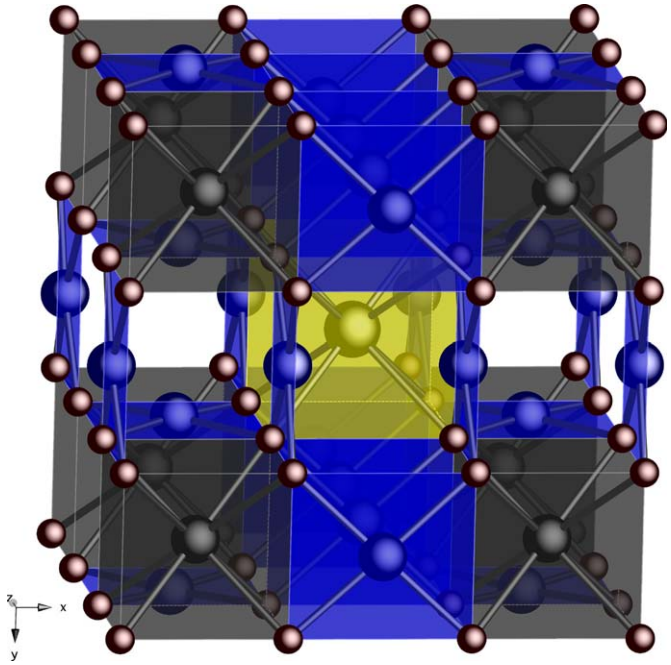

Fig. 15. Crystal structure of the ordered $LnNaPd_6O_8$ (Ln = Tb–Lu, Y) palladates. PdO_4 square planes are blue, NaO_8 cubes are yellow, LnO_8 cubes are gray, and oxygen atoms are red spheres. (For interpretation of the references to color in this figure legend, the reader is referred to the web version of this article.)

hydroxide fluxes. The reactions were carried out in sealed silver tubes at 700 °C over the period of 24 h. Single crystals formed as black cubes with crystal structure related to the APd_3O_4 (A = Ca, Sr) phases [32,143,151,152], where essentially the unit cell was doubled to yield the generic formula $A_2Pd_6O_8$. On the A-site, the substitution of one trivalent lanthanide cation and one monovalent sodium cation in place of two divalent alkaline earth metal cations occurred. The crystal structure consists of slabs of LnO_8 and NaO_8 cubes bridged together by PdO_4 square planes as shown in Fig. 15. The Ln and Na atoms are disordered within the slabs in all cases except in $LuNaPd_6O_8$, where a 1:1 ordered arrangement of LnO_8 and NaO_8 cubes is achieved. The amount of A-site disorder decreases as the ionic radius of the lanthanide cation decreases from Tb–Lu.

4.3. Oxides of platinum

4.3.1. $(Ln_2Na)NaPtO_6$

Single crystals of $(Ln_2Na)NaPtO_6$ [153,154] were grown from an acidic sodium hydroxide melts at 700 °C for 12 h in a silver crucible covered loosely with a silver lid. The compounds crystallize in the $R\bar{3}c$ space group and are $m = 0$, $n = 1$ (or $A_3A'BO_6$) members of the $A_{3n+3m}A'_nB_{3m+n}O_{9m+6n}$ family of 2H-perovskite related oxides [2]. Interestingly, $(La_2Na)NaPtO_6$ was the first example of an oxide of this structure type having a lanthanide cation (La^{3+}) on the A-site, where previously only divalent alkaline earth cations were found on the A-site.

The crystal structure of $(Ln_2Na)NaPtO_6$ consists of infinite chains of alternating face-shared $[NaO_6]$ trigonal prisms and $[PtO_6]$ octahedra as shown in Fig. 16. The structure is derived from the hexagonal stacking of close packed $[(Ln_2Na)NaO_6]$ layers with the subsequent filling of the generated octahedral sites by the Pt atoms. The polyhedral chains run along [001] and are separated from each other by six spiral chains of distorted $[(La/Na)O_8]$ square antiprisms.

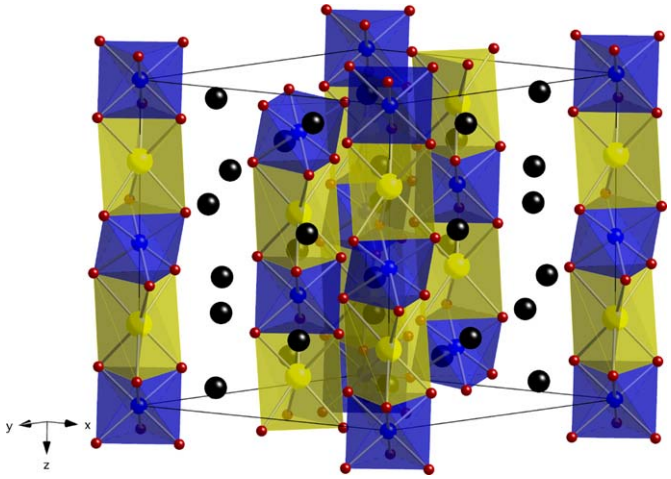

Fig. 16. The crystal structure of the 2H-related perovskite, $(La_2Na)NaPtO_6$. PtO_6 octahedra are shown in blue, NaO_6 distorted trigonal prisms in yellow, La(1)/Na(1) atoms are represented as black spheres, and oxygen atoms are red spheres. (For interpretation of the references to color in this figure legend, the reader is referred to the web version of this article.)

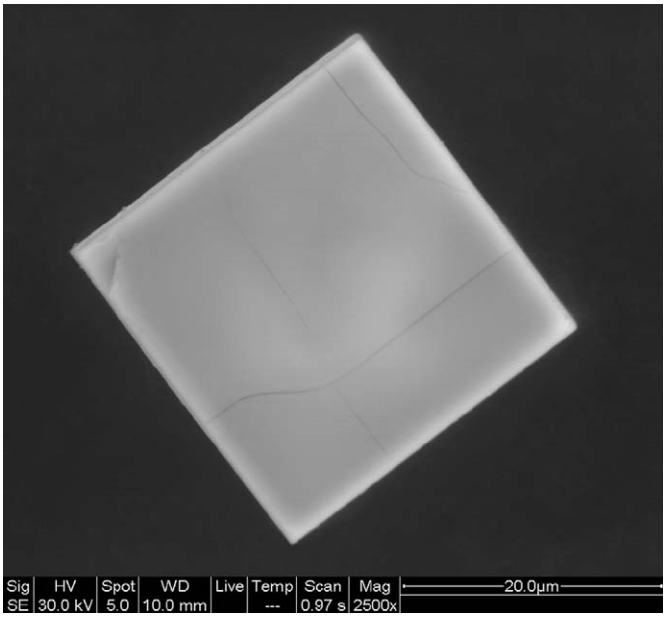

Fig. 17. Scanning electron micrograph of a single crystal of $K_4[Sm_6Pt_2O_{15}]$.

4.3.2. $K_4Ln_6Pt_2O_{15}$

Single crystals of the $K_4Ln_6Pt_2O_{15}$ (Ln = La, Pr, Nd, Sm–Gd) [155] platinates were grown from reactive potassium hydroxide flux reactions. In the case of $K_4La_6Pt_2O_{15}$, $K_4La_4Nd_2Pt_2O_{15}$, and $K_4Nd_6Pt_2O_{15}$, the crystal quality was improved by adding potassium fluoride to the reaction, which acted as a mineralizing agent. The crystals of $K_4Ln_6Pt_2O_{15}$ (Ln = La, Pr, Nd, Sm–Gd) formed as cubes or plates varying in colors of red-orange ($K_4La_6Pt_2O_{15}$), black ($K_4Pr_6Pt_2O_{15}$), blue-green ($K_4Nd_6Pt_2O_{15}$), yellow ($K_4Sm_6Pt_2O_{15}$) (Fig. 17), brown ($K_4Eu_6Pt_2O_{15}$), and orange ($K_4Gd_6Pt_2O_{15}$).

The structure of $K_4Ln_6Pt_2O_{15}$ (Ln = La, Pr, Nd, Sm–Gd) consists of a crystallographically well-behaved Ln–Pt–O framework permeated by channels of disordered atoms along [100] and equivalent directions (Fig. 18). This three-dimensional Ln–Pt–O framework is anionic, with composition and charge of $[Ln_6Pt_2O_{15}]^{4-}$. Within the channels in the framework, an essentially continuous distribution of electron density was observed. The $[Ln_6Pt_2O_{15}]^{4-}$ framework

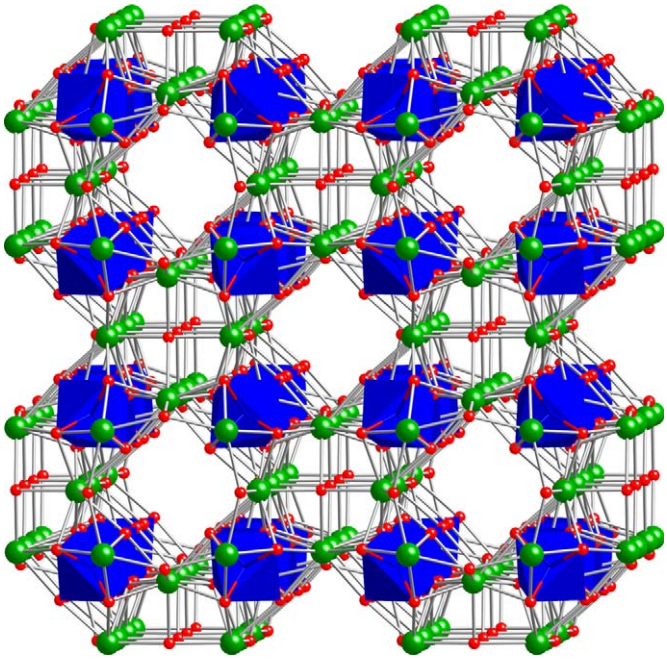

Fig. 18. Crystal structure of the $[La_6Pt_2O_{15}]^{4-}$ framework viewed down the *c*-axis. PtO_6 octahedra are shown in blue, lanthanum ions in green, and oxygen ions in red. Disordered potassium ions in the channels are not shown. (For interpretation of the references to color in this figure legend, the reader is referred to the web version of this article.)

consists of linked building blocks that are reminiscent of sodalite cages. Each such cage contains eight PtO_6 octahedra that are surrounded by 36 *Ln* atoms, 24 of which (6×4) are shared with the six surrounding cages. This leaves a cubic $Ln_{12}Pt_8$ core consisting of 8 Pt atoms at the corners and 12 *Ln* atoms roughly in the middle of each cube edge, thereby bridging adjacent Pt atoms. In the core, each Pt is in an octahedral PtO_6 environment, while each *Ln* is in a distorted bicapped trigonal prismatic LnO_8 coordination environment. The inside of each channel is "lined" with oxygen atoms that coordinate to the cations in the channel that provide charge balance for the $[Ln_6Pt_2O_{15}]^{4-}$ framework. The *Ln*–Pt–O cages connect in 3D to form channels in the *a*, *b*, and *c* directions; at each of the six junctions, four lanthanide and four oxygen atoms are shared.

4.4. Oxides of rhodium

4.4.1. $La_{2.47}Na_{1.53}RhO_6$

Single crystals of the 2H-related perovskite, $La_{2.47}Na_{1.53}RhO_6$ [154], were grown from a reactive sodium hydroxide flux reaction at 700 °C in a silver crucible covered loosely with a silver lid. The compound crystallizes in the trigonal space group $R\bar{3}c$ with the Kd_4CdCl_6 structure and crystal morphology resembling a hexagonal plate.

$La_{2.47}Na_{1.53}RhO_6$ is a lanthanide containing $m = 0$, $n = 1$ (or $A_3A'BO_6$) member of the $A_{3n+3m}A'_nB_{3m+n}O_{9m+6n}$ family of 2H-perovskite related oxides [2] and is isostructural to $(La_2Na)NaPtO_6$ [153]. There are very few examples of $A_3A'BO_6$ type compounds containing rhodium synthesized from a hydroxide flux and include only Sr_3LiRhO_6 and Sr_3NaRhO_6 [15]. The crystal structure consists of infinite chains of alternating face-shared $[NaO_6]$ trigonal prisms and $[RhO_6]$ octahedra as shown in Fig. 19. The structure is derived from the hexagonal stacking of close packed $[(Ln_2Na)NaO_6]$ layers with the subsequent filling of the generated octahedral sites by the Rh atoms. The polyhedral chains run along

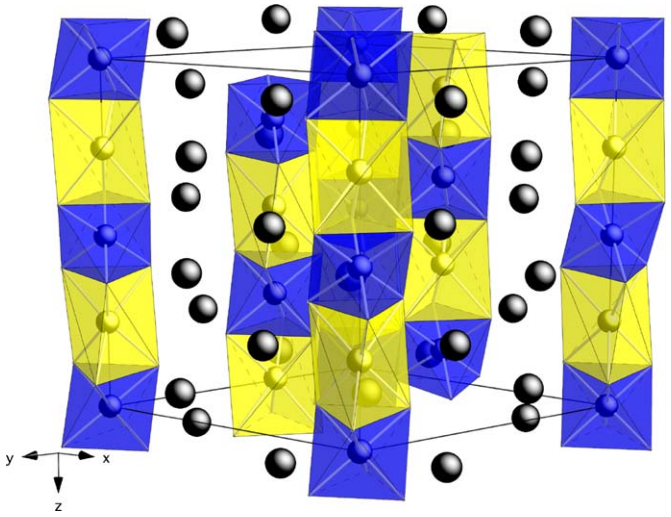

Fig. 19. The crystal structure of the 2H-related perovskite, $La_{2.47}Na_{1.53}RhO_6$. RhO_6 octahedra are shown in blue, NaO_6 distorted trigonal prisms in yellow and La(1)/Na(1) atoms are represented as black spheres. (For interpretation of the references to color in this figure legend, the reader is referred to the web version of this article.)

[001] and are separated from each other by six spiral chains of distorted $[(La/Na)O_8]$ square antiprisms.

5. Conclusions and general considerations

We have attempted to provide a detailed synopsis of the experimental considerations and procedures essential to working with molten hydroxide fluxes for crystal growth and simultaneously to summarize the results we have obtained from our study of the reactivity of alkali, lanthanide, and platinum group metals in molten hydroxides (Table 5). There are, however, some additional practical considerations that warrant mentioning. In virtually all cases, reaction conditions have to be systematically optimized for yield, phase purity and crystal quality. Thus, it is at times necessary to grow high quality crystals in low yield for use in single crystal X-ray diffraction and lower quality crystals in greater yield for physical property measurements.

Among these issues, perhaps the most important one concerns the yield of such crystal growth reactions where, not surprisingly, the results are unique to each specific reaction. Yields can vary from essentially 100%, where all reagents are converted into crystals, to only a few crystals when most of the reagents remain in the flux. In the latter instances, adjusting the concentrations and heating profiles in order to influence nucleation and growth, will typically improve yields, although not necessarily to 100%. Nonetheless, it is rare to find a reaction where one cannot improve the yield to the point where it is possible to obtain sufficient quantities of crystals for physical characterization.

Phase purity is another important aspect and conditions often have to be adjusted to favor the formation of only the desired product phase. Typically this involves changing the dwell temperature, which can become a trade-off between yield, phase purity and crystal quality. The addition of mineralizers, such as KF, into the flux also can have profound effects on crystal yield and crystal quality, as mineralizers can directly affect the dissolution process of the starting materials. Not all mineralizers work for all elements and, hence, it is necessary to use general coordination chemistry principles to guide the choice of the mineralizer.

Another important issue addresses the question of whether it is possible to prepare the material via a solid-state reaction, now

Table 5
List of complex platinum group metal oxides synthesized from hydroxide fluxes.

Phase	Flux	Ref.	Phase	Flux	Ref.
La_2LiIrO_6	LiOH	[85]	$SmKPdO_3$	KOH	[140]
Pr_2LiIrO_6	LiOH/KOH	[85]	$EuKPdO_3$	KOH	[140]
Nd_2LiIrO_6	LiOH/KOH	[85]	$GdKPdO_3$	KOH	[140]
Sm_2LiIrO_6	LiOH/KOH	[85]	$TbNaPd_6O_8$	NaOH	[150]
Eu_2LiIrO_6	LiOH/KOH	[85]	$DyNaPd_6O_8$	NaOH	[150]
La_2NaIrO_6	NaOH	[81]	$HoNaPd_6O_8$	NaOH	[150]
Pr_2NaIrO_6	NaOH	[81]	$ErNaPd_6O_8$	NaOH	[150]
Nd_2NaIrO_6	NaOH	[81]	$TmNaPd_6O_8$	NaOH	[150]
Sm_2NaIrO_6	NaOH/CsOH	[86]	$YbNaPd_6O_8$	NaOH	[150]
$La_{2.5}K_{1.5}IrO_7$	KOH	[104]	$LuNaPd_6O_8$	NaOH	[150]
$La_9RbIr_4O_{24}$	RbOH	[105]	$YNaPd_6O_8$	NaOH	[150]
$Nd_2K_2IrO_7$	KOH	[124]	$CaPd_3O_4$	KOH	[139]
$Sm_2K_2IrO_7$	KOH	[124]	$SrPd_3O_4$	KOH	[139]
Pr_3IrO_7	KOH, RbOH	[90]	$(La_2Na)NaPtO_6$	NaOH	[153]
Nd_3IrO_7	KOH, RbOH	[90]	$(Nd_2Na)NaPtO_6$	NaOH	[154]
Sm_3IrO_7	KOH, RbOH	[90]	$La_4K_6Pt_2O_{15}$	KOH/KF	[155]
Eu_3IrO_7	KOH, RbOH	[90]	$Pr_4K_6Pt_2O_{15}$	KOH/KF	[155]
$Gd_{0.96}Na_{1.04}IrO_4$	NaOH/CsOH	[117]	$Nd_4K_6Pt_2O_{15}$	KOH/KF	[155]
$Tb_{0.93}Na_{1.07}IrO_4$	NaOH/CsOH	[117]	$Sm_4K_6Pt_2O_{15}$	KOH/KF	[155]
$Dy_{0.94}Na_{1.06}IrO_4$	NaOH/CsOH	[117]	$Eu_4K_6Pt_2O_{15}$	KOH/KF	[155]
$Ho_{0.90}Na_{1.10}IrO_4$	NaOH/CsOH	[117]	$Gd_4K_6Pt_2O_{15}$	KOH/KF	[155]
$Er_{0.75}Na_{1.25}IrO_4$	NaOH/CsOH	[117]	Sr_3LiRhO_6	LiOH/KOH	[15]
$Y_{0.92}Na_{1.08}IrO_4$	NaOH/CsOH	[117]	Sr_3NaRhO_6	LiOH/NaOH	[15]
$Ba_3LiIr_2O_9$	KOH/LiOH	[76]	$La_{2.47}Na_{1.53}RhO_6$	NaOH	[154]
$Ba_3NaIr_2O_9$	NaOH	[76]	$Ba_7Li_3Ru_4O_{20}$	KOH/LiOH	[77]
$Ba_{3.44}K_{1.56}IrO_{10}$	KOH	[76]	$Ba_4NaRu_3O_{12}$	NaOH	[77]
La_2LiOsO_6	LiOH/KOH	[84]	$Ba_3LiRu_2O_9$	KOH/LiOH	[74]
Pr_2LiOsO_6	LiOH/KOH	[84]	$Ba_3NaRu_2O_9$	NaOH	[74]
Nd_2LiOsO_6	LiOH/KOH	[84]	La_2NaRuO_6	NaOH	[83]
Sm_2LiOsO_6	LiOH/KOH	[84]	Pr_2NaRuO_6	NaOH	[83]
La_2NaOsO_6	NaOH	[82]	Nd_2NaRuO_6	NaOH	[83]
Pr_2NaOsO_6	NaOH	[82]	Sm_3RuO_7	NaOH	[89]
Nd_2NaOsO_6	NaOH	[82]	Eu_3RuO_7	NaOH	[89]
Sm_3OsO_7	NaOH	[88]	$Pr_{14}Na_3Ru_6O_{30}$	NaOH	[102]
Eu_3OsO_7	NaOH	[88]	$Nd_{14}Na_3Ru_6O_{30}$	NaOH	[102]
Gd_3OsO_7	NaOH	[88]	$Nd_5Ru_2O_{12}$	KOH	[99]
Ba_2LiOsO_6	LiOH	[78]	$Sm_5Ru_2O_{12}$	NaOH	[99]
Ba_2NaOsO_6	NaOH	[78]	$Eu_5Ru_2O_{12}$	KOH	[99]
$Ba_3LiOs_2O_9$	LiOH	[75]	$Gd_5Ru_2O_{12}$	NaOH	[99]
$Ba_3NaOs_2O_9$	NaOH	[75]	$Tb_5Ru_2O_{12}$	KOH	[99]
$LaKPdO_3$	KOH	[140]	$Sr_{18}Ru_{1.9}Bi_{4.1}O_{33}$	$KOH/Sr(OH)_2$	[17]
$PrKPdO_3$	KOH	[140]	Sr_3LiRuO_6	KOH/LiOH	[72]
$PrKPd_{0.86}Cu_{0.14}O_3$	KOH	[140]	Sr_3LiRhO_6	LiOH/KOH	[15]
$NdKPdO_3$	KOH	[140]	Sr_3NaRhO_6	LiOH/NaOH	[15]

that the composition is known. This typically depends on the relative stability of the product vs. other stable phases that will form at high temperatures. A quick test of the thermal stability of the product can indicate the likelihood of being able to obtain the same composition by a high temperature solid-state reaction. If the material undergoes phase transition/decomposition at temperatures low relative to what is typically needed for a solid-state reaction, then the odds of being able to synthesize the material by a solid-state route are low. Also, if the crystal structure contains channels, even if thermally stable, it is rare that high temperature reactions will succeed, as they tend to yield more dense phases. In such cases it may be necessary to prepare multiple batches of crystals if greater quantities are needed. Thus, while it is often possible to prepare the same materials by a solid-state route, it is unfortunately not always the case.

A final topic concerns the issue of a reactive vs. a non-reactive flux, in this case, the potential incorporation of alkali metals. This topic is closely related to the complexity of the target oxide. One approach to obtaining complex oxides containing four or more elements is to choose reagents that under the reaction conditions will take on different oxidation states and that will be of different sizes with different coordination environment preferences. This will avoid two elements substituting for one another on the same crystallographic site and encourage each element to play a unique role in the final structure. Clearly, the alkali metals can fulfill such a role and, by being part of the flux, they are present in large quantities.

To predict the reactivity of a flux is problematic, but some general guidelines can be found. For example, one can hypothesize that when a very stable structure type forms that does not accommodate alkali metals, as is the case with many ternary phases, the flux will be non-reactive. But, when one creates conditions where entirely new structure types form, as is the case for many quaternary and most penternary phases, it becomes likely that the alkali metal will play a part in its formation and be incorporated. This is supported by the compositions we report here, where alkali metals are incorporated into most element rich compounds. Of course there are many known ternary phases containing alkali metals; however, since they are known, they are typically not reported in crystal growth experiments involving hydroxide fluxes and, in fact, conditions are often adjusted to avoid their formation.

In summary, it can be safely stated that molten hydroxides are an excellent medium for the crystal growth of complex lanthanide-containing platinum group metal oxides and can greatly aid in the discovery of new complex oxide materials. The utility of molten hydroxides as a solvent is certainly not limited to the crystal growth of platinum group metal containing oxides and, although not covered in this review, their usefulness for the crystal growth of early transition metal, main group metal and actinide metal containing oxides has been demonstrated by us and others.

Acknowledgments

We gratefully acknowledge the continued support for this research by the National Science Foundation for well over a decade, most recently through Grants DMR:0450103 and DMR:0804209.

References

[1] D.M. Giaquinta, H.-C. zur Loye, Chem. Mater. 6 (1994) 365.
[2] K.E. Stitzer, J. Darriet, H.C. zur Loye, Curr. Opin. Solid State Mater. Sci. 5 (2001) 535.
[3] K.R. Poeppelmeier, Chem. Mater. 10 (1998) 2577.
[4] F.J. DiSalvo, Science 247 (1990) 649.
[5] M. Jansen, Angew. Chem. Int. Ed. 41 (2002) 3746.
[6] M. Jansen, J.C. Schön, Angew. Chem. Int. Ed. 45 (2006) 3406.
[7] R.D. Shannon, Acta Crystallogr. 32 (1976) 751.
[8] V.M. Goldschmidt, Mat. Nat. Kl. 2 (1926) 117.
[9] D. Elwell, H.J. Scheel, Crystal Growth from High-Temperature Solutions, Academic Press, New York, 1975.
[10] B. Tremillon, Rev. Chim. Min. 3 (1966) 767.
[11] B. Tremillon, Reactions in Solutions: An Applied Analytical Approach, Wiley, New York, 1997, p. 554.
[12] B. Tremillon, G. Picard, Ec. Natl. Super. Chim. Paris 82 (1976) 273.
[13] W. Sundermeyer, Angew. Chem. 77 (1965) 241.
[14] J.L. Luce, A.M. Stacy, Chem. Mater. 9 (1997) 1508.
[15] B.A. Reisner, A.M. Stacy, J. Am. Chem. Soc. 120 (1998) 9682.
[16] S.W. Keller, V.A. Carlson, D. Sanford, F. Stenzer, A.M. Stacy, G.H. Kwei, M.J. Alario-Franco, J. Am. Chem. Soc. 116 (1994) 8070.
[17] M.S. Martin-Gonzalez, J.L. Delattre, A.M. Stacy, J. Solid State Chem. 173 (2003) 203.
[18] P.D. VerNooy, M.A. Dixon, F.J. Hollander, A.M. Stacy, Inorg. Chem. 29 (1990) 2837.
[19] L.N. Marquez, S.W. Keller, A.M. Stacy, Chem. Mater. 5 (1993) 761.
[20] S.L. Stoll, A.M. Stacy, C.C. Torardi, Inorg. Chem. 33 (1994) 2761.
[21] D. Sandford, L.N. Marquez, A.M. Stacy, Appl. Phys. Lett. 67 (1995) 422.
[22] P.D. VerNooy, A.M. Stacy, J. Solid State Chem. 95 (1991) 270.
[23] J.L. Delattre, A.M. Stacy, V.G. Young, G.J. Long, R. Hermann, F. Grandjean, Inorg. Chem. 41 (2002) 2834.
[24] P.M. Keane, D.G. Hinks, U. Geiser, J.M. Williams, Physica C 226 (1994) 353.
[25] H. Flood, T. Forland, Acta Chem. Scand. 1 (1947) 592.
[26] H.Z. Lux, Electrochem. Angew. Phys. Chem. 45 (1939) 303.

[27] J. Goret, Bull. Soc. Chim. (1964) 1074.
[28] B. Tremillon, R.G. Doisneau, J. Chim. Phys. Phys. Chim. Biol. 71 (1974) 1379.
[29] B. Tremillon, Pure Appl. Chem. 25 (1971) 395.
[30] H. Lux, R. Kuhn, T. Niedermaier, Z. Anorg. Allg. Chem. 298 (1959) 285.
[31] G. Wehrum, R. Hoppe, Z. Anorg. Allg. Chem. 617 (1992) 45.
[32] V.H.-D. Wasel-Nielen, R. Hoppe, Z. Anorg. Allg. Chem. 375 (1970) 209.
[33] D. Fischer, R. Hoppe, K.M. Mogare, M. Jansen, Z. Naturforsch. B Chem. Sci. 60 (2005) 1113.
[34] R. Hoppe, Z. Anorg. Allg. Chem. 630 (2004) 2384.
[35] R. Hoppe, K. Bernet, A. Moeller, Z. Anorg. Allg. Chem. 629 (2003) 1285.
[36] A. Moeller, M.A. Hitchman, E. Krausz, R. Hoppe, Inorg. Chem. 34 (1995) 2684.
[37] K. Mader, R. Hoppe, J. Alloys Compd. 206 (1994) 271.
[38] M. Schlaeger, R. Hoppe, Austral. J. Chem. 45 (1992) 1427.
[39] K. Mader, R. Hoppe, J. Alloys Compd. 183 (1992) 198.
[40] D. Fischer, R. Hoppe, J. Alloys Compd. 183 (1992) 187.
[41] J. Birx, R. Hoppe, Z. Anorg. Allg. Chem. 597 (1991) 19.
[42] D. Fischer, R. Hoppe, Angew. Chem. 102 (1990) 835.
[43] S. Voigt, R. Hoppe, J. Less-Common Metals 156 (1989) 97.
[44] D. Schuldt, R. Hoppe, Z. Anorg. Allg. Chem. 575 (1989) 77.
[45] R. Hofmann, R. Hoppe, Z. Anorg. Allg. Chem. 569 (1989) 31.
[46] R. Hoppe, H.P. Mueller, Z. Anorg. Allg. Chem. 551 (1987) 136.
[47] R. Wolf, R. Hoppe, J. Solid State Chem. 70 (1987) 12.
[48] R. Wolf, R. Hoppe, Rev. Chim. Min. 23 (1986) 828.
[49] E. Seipp, R. Hoppe, Z. Naturforsch. B 41B (1986) 1513.
[50] R. Hofmann, B. Nowitzki, R. Hoppe, Z. Naturforsch. B 40B (1985) 1441.
[51] M. Serafin, R. Hoppe, Rev. Chim. Min. 20 (1983) 214.
[52] W. Burow, R. Hoppe, Angew. Chem. 91 (1979) 71.
[53] M. Sofin, E.-M. Peters, M. Jansen, Solid State Sci. 6 (2004) 339.
[54] G. Kramer, E. Hagele, N. Wagner, M. Jansen, Z. Anorg. Allg. Chem. 622 (1996) 1027.
[55] G. Kramer, M. Jansen, J. Solid State Chem. 114 (1995) 206.
[56] L. Wulff, H. Mueller-Buschbaum, Z. Naturforsch. B B53 (1998) 283.
[57] D. Schlueter, H. Mueller-Buschbaum, J. Alloys Compd. 191 (1993) 305.
[58] S. Frenzen, H. Müller-Buschbaum, Z. Naturforsch. B 50b (1995) 581.
[59] S. Frenzen, H. Mueller-Buschbaum, Z. Naturforsch. B 51 (1996) 1204.
[60] S. Frenzen, H. Mueller-Buschbaum, Z. Naturforsch. B 51 (1996) 822.
[61] S. Frenzen, H. Mueller-Buschbaum, Z. Naturforsch. B 51 (1996) 485.
[62] S. Frenzen, H. Mueller-Buschbaum, Z. Naturforsch. B 51 (1996) 225.
[63] J. Weinreich, H. Mueller-Buschbaum, Z. Anorg. Allg. Chem. 619 (1993) 537.
[64] G. Tams, H. Mueller-Buschbaum, Z. Anorg. Allg. Chem. 617 (1992) 19.
[65] J. Weinreich, H. Mueller-Buschbaum, Z. Anorg. Allg. Chem. (1992) 27.
[66] J. Weinreich, H. Mueller-Buschbaum, J. Alloys Compd. 184 (1992) 187.
[67] H. Lux, T. Niedermaier, Z. Anorg. Allg. Chem. 282 (1955) 196.
[68] H. Lux, E. Renauer, E. Betz, Z. Anorg. Allg. Chem. 310 (1961) 305.
[69] L.C. Beavis, Rev. Sci. Instr. 43 (1971) 122.
[70] R.A. Outlaw, S.N. Sankaran, G.B. Hoflund, M.R. Davidson, J. Mater. Res. 3 (1988) 1378.
[71] J.B. Claridge, R.C. Layland, W.H. Henley, H.-C. zur Loye, Chem. Mater. 11 (1999) 1376.
[72] M.J. Davis, M.D. Smith, K.E. Stitzer, H.C. zur Loye, J. Alloys Compd. 351 (2003) 95.
[73] P. Núñez, S. Trail, H.-C. zur Loye, J. Solid State Chem. 130 (1997) 35.
[74] K.E. Stitzer, M.D. Smith, W.R. Gemmill, H.-C. zur Loye, J. Am. Chem. Soc. 124 (2002) 13877.
[75] K.E. Stitzer, A. El Abed, M.D. Smith, M.J. Davis, S.J. Kim, J. Darriet, H.-C. zur Loye, Inorg. Chem. 42 (2003) 947.
[76] S.J. Kim, M.D. Smith, J. Darriet, H.C. zur Loye, J. Solid State Chem. 177 (2004) 1493.
[77] K.E. Stitzer, W.R. Gemmill, M.D. Smith, H.-C. zur Loye, J. Solid State Chem. 175 (2003) 39.
[78] K.E. Stitzer, M.D. Smith, H.-C. zur Loye, Solid State Sci. 4 (2002) 311.
[79] S. Yonezawa, Y. Muraoka, Y. Matsushita, Z. Hiroi, J. Phys. Soc. Jpn. 74 (2004) 819.
[80] S. Yonezawa, Y. Muraoka, Y. Matsushita, Z. Hiroi, J. Phys. Condens. Mater. 16 (2004) L9.
[81] M.J. Davis, S.J. Mugavero III, K.I. Glab, M.D. Smith, H.-C. zur Loye, Solid State Sci. 5 (2004) 413.
[82] W.R. Gemmill, M.D. Smith, R. Prozorov, H.-C. zur Loye, Inorg. Chem. 44 (2005) 2639.
[83] W.R. Gemmill, M.D. Smith, H.-C. zur Loye, J. Solid State Chem. 177 (2004) 3560.
[84] W.R. Gemmill, M.D. Smith, H.C. zur Loye, J. Solid State Chem. 179 (2006) 1750.
[85] S.J. Mugavero III, M.D. Smith, H.-C. zur Loye, J. Solid State Chem. 178 (2004) 200.
[86] S.J. Mugavero III, I.V. Puzdrjakova, M.D. Smith, H.-C. zur Loye, Acta Crystallogr. E E61 (2005) i3.
[87] R.M. Mitchell, Perovskites: Modern and Ancient, Almaz Press, Thunder Bay, 2002.
[88] W.R. Gemmill, M.D. Smith, Y.A. Mozharivsky, G.J. Miller, H.-C. zur Loye, Inorg. Chem. 44 (2005) 7047.
[89] W.R. Gemmill, M.D. Smith, H.-C. zur Loye, Inorg. Chem. 43 (2004) 4254.
[90] W.R. Gemmill, Thesis, University of South Carolina, 2006.
[91] W.R. Gemmill, M.D. Smith, H.-C. zur Loye, J. Chem. Crystallogr. 37 (2007) 793.
[92] J.G. Allpress, H.J. Rossell, J. Solid State Chem. 27 (1979) 105.
[93] H. Nishime, M. Wakeshima, Y. Hinatsu, J. Solid State Chem. 177 (2004) 739.
[94] J.E. Greedan, N.P. Raju, A. Wegner, P. Gougeon, J. Padiou, J. Solid State Chem. 129 (1997) 320.
[95] D. Harada, Y. Hinatsu, J. Solid State Chem. 158 (2001) 245.
[96] D. Harada, Y. Hinatsu, J. Solid State Chem. 164 (2002) 163.
[97] D. Harada, Y. Hinatsu, Y. Ishii, J. Phys. Condens. Mater. 13 (2001) 10825.
[98] H. Nishimine, M. Wakeshima, D. Harada, J. Solid State Chem. 177 (2004) 739.
[99] M. Bharathy, W.R. Gemmill, A.H. Fox, J. Darriet, M.D. Smith, J. Hadermann, M.S. Remy, H.-C. zur Loye, J. Solid State Chem. 182 (2009) 1164.
[100] L. Chi, J.F. Britten, J.E. Greedan, J. Solid State Chem. 172 (2003) 451.
[101] C.C. Torardi, C. Fecketter, W.H. McCarrol, F.J. DiSalvo, J. Solid State Chem. 60 (1985) 332.
[102] W.R. Gemmill, M.D. Smith, H.-C. zur Loye, Inorg. Chem. 46 (2007) 2132.
[103] P. Khalifah, Q. Huang, D.M. Ho, H.W. Zandbergen, R.J. Cava, J. Solid State Chem. 155 (2000) 189.
[104] S.J. Mugavero III, M.D. Smith, H.-C. zur Loye, J. Solid State Chem. 178 (2005) 3176.
[105] S.J. Mugavero III, M.D. Smith, H.C. zur Loye, Inorg. Chem. 45 (2006) 946.
[106] L. Bie, J. Lin, Y. Wang, C.-K. Loong, Inorg. Chem. Commun. 5 (2002) 966.
[107] L. Bie, Y. Wang, J. Lin, C.-K. Loong, J.W. Richardson Jr., L. You, C. Dong, Chem. Mater. 15 (2003) 516.
[108] F. Grasset, C. Dusserrat, J. Darriet, J. Mater. Chem. 7 (1997) 1911.
[109] F. Grasset, M. Zakhour, J. Darriet, J. Alloys Compd. 287 (1999) 25.
[110] Y. Wang, J. Lin, Y. Du, R. Qin, B. Han, C. Loong, Angew. Chem. Int. Ed. 39 (2000) 2730.
[111] Y.-X. Wang, L.-J. Bie, Y. Du, J.-H. Lin, C.-K. Loong, J.W. Richardson Jr., L.-P. You, J. Solid State Chem. 177 (2004) 65.
[112] S.G. Ebbinghaus, J. Solid State Chem. 177 (2004) 817.
[113] T. Gotzfried, A. Reller, S.G. Ebbinghaus, Inorg. Chem. 44 (2005) 6550.
[114] T. Gotzfried, A. Reller, S.G. Ebbinghaus, Solid State Sci. 6 (2004) 1205; P. Lunkenheimer, T. Goetzfried, R. Fichtl, S. Weber, T. Rudolf, A. Loidl, A. Reller, S.G.J. Ebbinghaus, Solid State Chem. 179 (2006) 3965.
[115] S.G. Ebbinghaus, C. Erztoument, I. Marozau, J. Solid State Chem. 180 (2007) 3393.
[116] T.J. Hansen, R.B. Macquart, M.D. Smith, H.-C. zur Loye, Solid State Sci. 9 (2007) 785.
[117] S.J. Mugavero III, M.D. Smith, H.C. zur Loye, Solid State Sci. 9 (2007) 555.
[118] D. Babel, W. Rudorff, R. Tschopp, Z. Anorg. Allg. Chem. 347 (1966) 282.
[119] F.J.J. Dijksma, J.F. Vente, E. Frikkee, D.J.W. IJdo, Mater. Res. Bull. 28 (1993) 1145.
[120] C.L. McDaniel, S.J. Schneider, J. Solid State Chem. 4 (1972) 275.
[121] F. Rodi, D. Babel, Z. Anorg. Allg. Chem. 336 (1965) 17.
[122] R.F. Sarkozy, C.W. Moeller, B.L. Chamberland, J. Solid State Chem. 9 (1974) 242.
[123] M. Wakeshima, N. Taira, Y. Hinatsu, Y. Ishii, Solid State Commun. 125 (2003) 311.
[124] S.J. Mugavero III, M.D. Smith, W.-S. Yoon, H.C. zur Loye, Angew. Chem. Int. Ed. 48 (2009) 215–218.
[125] G. Demazeau, D.-Y. Jung, Eur. J. Solid State Inorg. Chem. 32 (1995) 383.
[126] G. Demazeau, D.-Y. Jung, A. Largeteau, C. Cros, J.H. Choy, J. Alloys Compd. 262–263 (1997) 191.
[127] D.-Y. Jung, P. Graveneau, G. Demazeau, Eur. J. Solid State Inorg. Chem. 30 (1993) 1025.
[128] O. Muller, R. Roy, Adv. Chem. Ser. 98 (1971) 28.
[129] M. Andersson, J. Grins, M. Nygren, J. Solid State Chem. 146 (1999) 428.
[130] J.P. Attfield, Acta Crystallogr. B 44 (1988) 563.
[131] J.P. Attfield, G. Ferey, J. Solid State Chem. 80 (1989) 286.
[132] K.T. Jacob, K.T. Lwin, Y. Waseda, Solid State Sci. 4 (2002) 205.
[133] P. Sonne, H. Muller-Buschbaum, Z. Anorg. Allg. Chem. 619 (1993) 1004.
[134] S. Schiffler, H. Muller-Buschbaum, J. Less-Common Metals 128 (1987) 117.
[135] S.-J. Kim, S. Lemaux, G. Demazeau, J.-Y. Kim, J.-H. Choy, J. Am. Chem. Soc. 123 (2001) 10413.
[136] Y. Wang, D. Walker, B.-H. Chen, B.A. Scott, J. Alloys Compd. 285 (1999) 98.
[137] A.W. Sleight, Mater. Res. Bull. 3 (1968) 699.
[138] G. Demazeau, I. Omeran, M. Pouchard, P. Hagenmuller, Mater. Res. Bull. 11 (1976) 1449.
[139] P.L. Smallwood, M.D. Smith, H.C. zur Loye, J. Cryst. Growth 216 (2000) 299.
[140] S.J. Mugavero III, M.D. Smith, H.C. zur Loye, Inorg. Chem. 46 (2007) 3116.
[141] N.N. Eremin, L.I. Leonyuk, V.S. Urusov, J. Solid State Chem. 158 (2001) 162.
[142] M. Hjorth, J. Hyldtoft, Acta Chem. Scand. 44 (1990) 516.
[143] Y. Laligant, A. Le Bail, G. Ferey, M. Hervvieu, B. Raveau, A. Wilkinson, A.K. Cheetham, Eur. J. Solid State Inorg. Chem. 25 (1988) 237.
[144] D.R. Lines, M.T. Weller, D.B. Currie, D.M. Ogborne, Mater. Res. Bull. 26 (1991) 223.
[145] Y. Nagata, T. Taniguchi, G. Tanaka, M. Satho, H. Samata, J. Alloys Compd. 346 (2002) 50.
[146] C.L. Teske, H. Muller-Buschbaum, Z. Anorg. Allg. Chem. 371 (1969) 325.
[147] C.L. Teske, H. Muller-Buschbaum, Z. Anorg. Allg. Chem. 379 (1970) 234.
[148] M.T. Weller, D.R. Lines, J. Solid State Chem. 82 (1989) 21.
[149] W. Wong-Ng, K.L. Davis, R.S. Roth, J. Am. Ceram. Soc. 71 (1988) 64.
[150] S.J. Mugavero III, M.D. Smith, H.C. zur Loye, Cryst. Growth Des. 8 (2008) 494.
[151] J. Waser, E.D. McClanahan Jr., J. Chem. Phys. 19 (1951) 413.
[152] R.C. Wnuk, T.R. Touw, B. Post, IBM J. (1964) 185.
[153] M.J. Davis, M.D. Smith, H.-C. zur Loye, Inorg. Chem. 42 (2003) 6980.
[154] R.B. Macquart, W.R. Gemmill, M.J. Davis, M.D. Smith, H.C. zur Loye, Inorg. Chem. 45 (2006) 4391.
[155] H.-C. zur Loye, T.J. Hansen, Q. Zhao, S.J. Mugavero III, R.L. Withers, M.D. Smith, Inorg. Chem. 48 (2009) 414–416.
[156] D.L. Perry, S.L. Phillips, S. L., in: Handbook of Inorganic Compounds, CRC Press, Orinda, CA, 1995.
[157] J.F. Vente, D.J.W. IJdo, Mater. Res. Bull. 26 (1991) 1255.